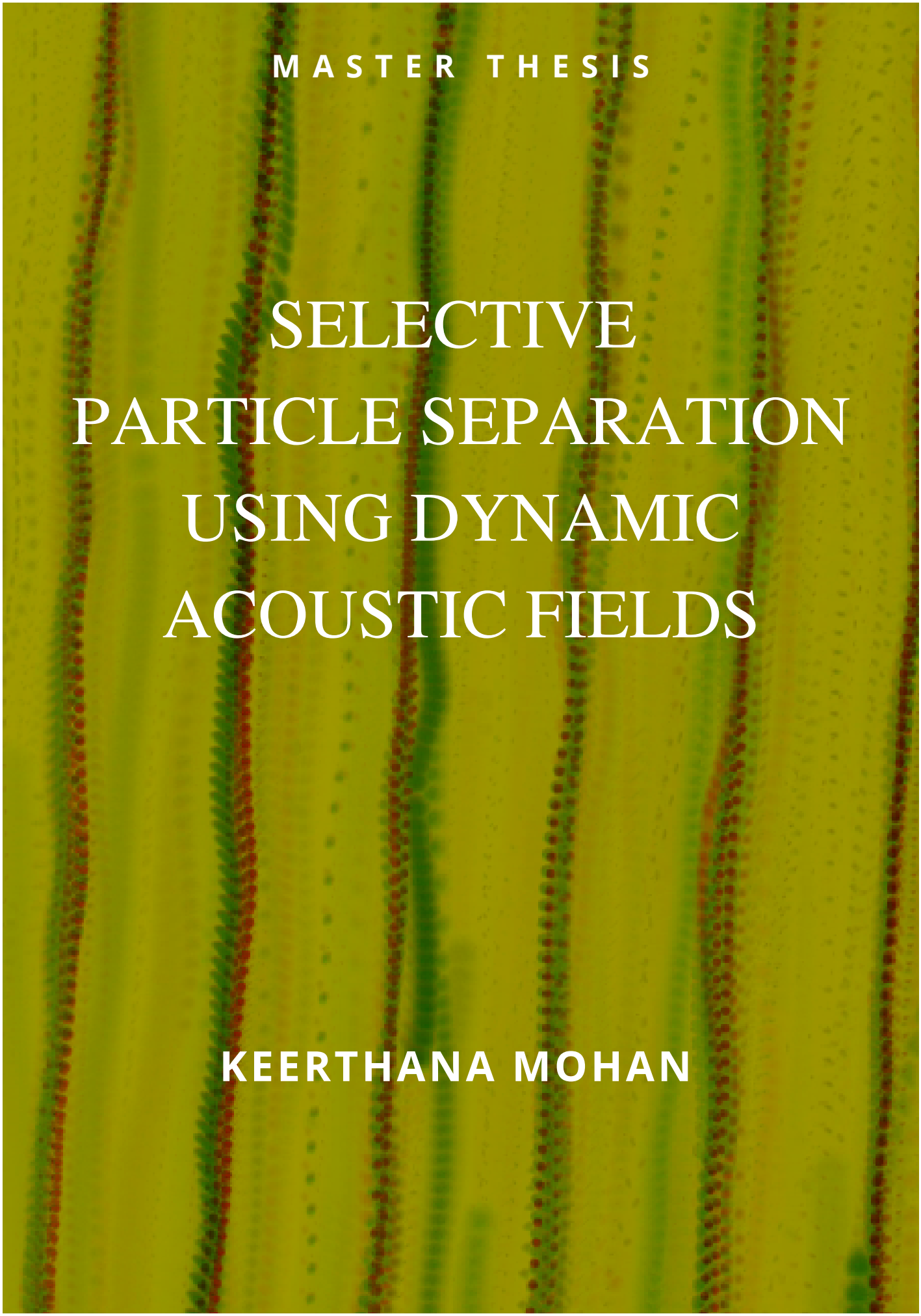

MASTER THESIS

SELECTIVE PARTICLE SEPARATION USING DYNAMIC ACOUSTIC FIELDS

KEERTHANA MOHAN

TU Delft

SELECTIVE PARTICLE SEPARATION USING DYNAMIC ACOUSTIC FIELDS

by

KEERTHANA MOHAN

in partial fulfilment of the requirements for the degree of

Master of Science
in Mechanical Engineering
at the Delft University of Technology,

To be defended publicly on Friday, September 25, 2020 at 14:00 hrs.

Student number:	4837509	
P&E Report number:	3031	
Thesis Committee:	Dr. ir. H. B. Eral,	TU Delft, Supervisor
	Prof. Dr. ir. J. T. Padding,	TU Delft
	Dr. H. Bazyar,	TU Delft
	Ir. M. H. Kandemir,	Wetsus & WUR, Daily Supervisor
	Dr. ir. D. R. Yntema,	Wetsus

TU Delft

ACKNOWLEDGEMENTS

I would first like to thank my Wetsus supervisor **Hakan Kandemir**, for giving me the opportunity to work on a topic very dear to me. Hakan was always available to bounce off ideas, discuss concepts and answer the stupidest of questions, and that is something I wish to imbibe. Hakan also patiently reviewed several versions of the thesis, pointing out minute things that could make it better, for which I am very grateful. I am also thankful to **Dr. ir. Doekle Yntema** for his insights on the working of transducers & other electronic components. I would also like to thank **Dr. ir. Burak Eral**, for consenting to be my supervisor from the University.

My gratitude goes to the technical team at Wetsus, **Jan Jurjen Salverda**, **Jan Tuinstra** in particular, who were quick to fix and build things whenever needed. My gratitude also to **Jan-Willem Schoonen** from the analytical lab, who helped every time I ran into trouble with the DIPA 2000 particle size analyser, which was quite often.

My thanks goes out to the wonderful friends I made at Wetsus, **Aishwarya** & **Nandini** in particular, with whom laughter & great company was always assured. With student interns changing every 3 months, I am very grateful to have had constant contact with **Ema**, **Daniel**, **Ivo** & **Zhan**, with whom fun and inane conversations were the order of the day. I am also very thankful for the countless other interactions with fellow interns, PhD students and Wetsus staff, who made my time at Wetsus happy and memorable. I would also like to thank my housemates at Keizerskroon 307 for the peaceful environment they helped create. I am especially grateful for their company during the Covid lockdown.

I would like to thank the closest friends I made at Netherlands: **Raj**, **Vasu** & **Madhu**. They have been there through the majority of my Masters journey. During my time in Leeuwarden, they constantly checked up on me and made sure I was doing well. Video calls and online games with them were especially invaluable during the Covid lockdown. My special thanks also to **Vasu** & **Suriya** for the many discussions on fluid mechanics and for helping out with questions I had. To my best friends from India: **Aarthi**, **Priya**, **Varun**, **Ram** & **Srini**, thank you for all the love, patience & the constant flood of messages you send.

To the people who have been a constant source of encouragement and support: **Phani** & **Kalpit**, I cannot emphasize enough, how grateful I am. You made this journey easier.

Last but not the least, my heartfelt gratitude to my family, who have always been my biggest cheerleaders. This thesis is dedicated to my sister, who serves as my inspiration, and my parents, whose belief and unconditional love & support has made me what I am today. I am eternally indebted to them.

Keerthana Mohan
Rotterdam, September 2020

ABSTRACT

Separation of particles from suspensions has been an integral part of many industrial, chemical and biological processes. Traditional methods such as sieving, flocculation, centrifugation etc. have many demerits. This has lead to an interest in unconventional separation methods that use physical properties of the particles. Acoustophoresis is one such method that has gained popularity in recent times. Acoustophoretic separation is based on the density contrast between the particles and the medium, as well as the size of the particles. A particle in a medium in which an acoustic field has been applied, experiences an acoustic force. This acoustic force is greater in standing waves than traveling waves, which is why acoustophoretic devices generally use standing wave fields. Particles with positive contrast factor are pushed to the pressure nodes; once the particles reach the nodes, they are trapped. If the medium is in flow, the particles also experience drag force. The interplay between the drag and the acoustic force forms the basis for separation. Standing wave fields can further be distinguished as static fields or dynamic acoustic fields (DAF). In a static field, the nodes are stationary, while in a DAF, there is movement of the nodes, caused by variation of source frequency. Here, the tendency of different-sized particles to follow the nodal movement gives rise to separation. DAF devices seem preferable when separation needs to be done on a larger scale.

In this thesis, two novel DAF devices were studied; one device works on the principle of frequency sweeping, while the other works on frequency modulation. Both devices are 3D printed, and have two inlets and two exits, with separation occurring in an acoustic chamber where the DAF acts. Both devices are multi-nodal & milli-fluidic. The samples to be separated consist of polyethylene particles of a continuous size distribution between 32-106 µm, dispersed in water. The devices were tested at a total channel flow rate of 1000 ml h^{-1} (Reynolds number of 20). The aim was to understand how varying the flow and acoustic field parameters affect the separation/filtration performance of the devices. This was done by defining a “threshold size” or the cut-off size at which the entire particle distribution is divided into two separate distributions. Flow and acoustic field parameters were adjusted to see how the threshold size increases/decreases.

The analysis for each device was done by a parametric study using Design of Experiments (DOE). First the available features (both design and operation) were studied and suitable parameters and their values were selected. The DOE was then designed, having 27 combinations of the values, each combination known as a ‘run’. Each run of the DOE was first simulated on an available 2D COMSOL model, followed by experimental validation. The DOE was then analysed using both theoretical and actual values, to find out the parameters that had the maximum effect on the threshold size, and their respective trends.

The thesis was carried out at **Wetsus, European centre of excellence for sustainable water technology**, at Leeuwarden.

Keywords: millifluidics, microparticles, dynamic acoustic field, size selective separation, filtration, frequency sweep, frequency modulation, inertial regime, parametric study

CONTENTS

List of Figures

List of Tables

NOMENCLATURE

0.1. SYMBOLS

x	Position in space (m)	
t	Time (s)	
P	Pressure variation in medium (Pa)	
P_0	Amplitude of pressure variation (Pa)	
v	Acoustic velocity (m s^{-1})	
λ	Wavelength (m)	
k	Wavenumber (m^{-1})	$\left[k = \frac{2\pi}{\lambda}\right]$
f	Frequency (Hz)	
ω	Angular frequency (rad s^{-1})	$[\omega = 2\pi f]$
ϵ	Angular frequency difference (Hz)	$[\epsilon = \omega_1 - \omega_0]$
Z	Acoustic Impedance (Pa s m^{-3})	$[z = P/v]$
ρ_w	Density of medium (kg m^{-3})	
μ_w	Viscosity of medium (N s m^{-2})	
c_w	Speed of sound in medium (m s^{-1})	$\left[c = \lambda f = \frac{\omega}{k}\right]$
T	Time period of sweep (s)	
S	Sweep rate (s^{-2})	$\left[S = \frac{\omega_1 - \omega_0}{T}\right]$
E_{ac}	Acoustic energy density (Pa)	$\left[E_{ac} = \frac{P_0^2}{4\rho_w c_w^2}\right]$
r_p, d_p	Particle radius, diameter (m)	
ρ_p	Density of particle (kg m^{-3})	
m_p	Mass of particle (kg)	
c_p	Speed of sound in particle (m s^{-1})	
ϕ	Acoustic contrast factor (-)	$\left[\phi = \frac{\rho_p + \frac{2}{3}(\rho_p - \rho_w)}{2\rho_p + \rho_w} - \frac{(\rho_w - c_w^2)}{3\rho_p c_p^2}\right]$

u_p	Particle Velocity ($m\,s^{-1}$)	
u_w	Fluid Velocity ($m\,s^{-1}$)	
u_r	Relative particle velocity ($m\,s^{-1}$)	$\left[u_r = (u_p - u_w)\right]$
D_h	Hydraulic diameter of channel (m)	$\left[D_h = \frac{4*Area}{Perimeter}\right]$
Re	Reynold's number (-)	$\left[Re = \frac{\rho_w D_h u_w}{\mu_w}\right]$
Re_p	Particle Reynold's number (-)	$\left[Re = \frac{\rho_w d_p u_r}{\mu_w}\right]$
C_d	Drag Coefficient (-)	$\left[C_d = \frac{24}{Re_p}\left(1 + 0.15Re_p^{0.687}\right)\right]$
F_{ac}	Acoustophoretic radiation force (N)	$\left[F_{ac}(x) = 4\pi r_p^3 k \phi E_{ac} \sin(2kx)\right]$
F_d	Drag force (N)	$\left[F_d = C_d . \frac{\pi}{4} d_p^2 . \frac{1}{2} \rho_w u_r^2\right]$
a	Acceleration of the particle ($m\,s^{-2}$)	
$\dot{V}_1$	Inlet particle stream ($ml\,h^{-1}$)	
$\dot{V}_2$	Inlet water stream ($ml\,h^{-1}$)	
$\dot{V}_3$	Transducer / higher frequency exit stream ($ml\,h^{-1}$)	
$\dot{V}_4$	Reflector / lower frequency exit stream ($ml\,h^{-1}$)	

0.2. ACRONYMS

ASF	Analytical SPLITT Fractionation	PLA	Polylactic acid
DAF	Dynamic Acoustic Field	PVA	Polyvinyl alcohol
DOE	Design of Experiments	CTAB	Cetyl Trimethyl Ammonium Bromide
EOM	Equation of Motion	LDPE	Low-density polyethylene
FFA	Free Flow Acoustophoresis	PMMA	Poly(methyl methacrylate)
LDV	Laser Doppler Vibrometer		
PSD	Particle Size Distribution		
SHM	Simple Harmonic Motion		
SPLITT	Split Flow Thin		

1

INTRODUCTION

1.1. ACOUSTOPHORETIC DEVICES

The use of acoustophoresis as an unconventional method of particle manipulation and separation has been prevalent in recent decades, with early separation devices used mainly in biological applications. Later research was extended to study separation of latex, glass, polystyrene beads etc., the applications for which need to be further explored. The advantage that acoustophoresis hold over other methods, even over other unconventional ones such as magnetophoresis or electrophoresis, is that additional properties such as electric charge or magnetism are not required. Particle manipulation in acoustophoresis relies only on physical properties such as density & size of the particle. There are some possible benefits offered by acoustophoresis, such as absence of fouling or clogging, no need for use of chemical reagents, no moving parts etc. Traditional separation devices are usually on mm scale in construction, and operate in the microfluidic range ($\dot{Vol} \sim \mu l\,min^{-1}$). These devices operate in the ultrasonic frequency range ($f \sim$ MHz), as a larger frequency would imply greater acoustic force that causes separation, and would also help prevent cavitation effects brought on at lower frequencies [5]. The devices mostly operate with a single pressure node in the middle of the channel. This node does not vary in space and hence is called a "static field".

The simplest static field devices are based on Free Flow Acoustophoresis (FFA). FFA devices usually consist of half wavelength resonators, with a pressure node at the centre of the chamber. The flow and acoustic field are perpendicular to each other; the larger particles move faster towards the nodes, while the smaller particles lag behind, or do not face enough acoustic force to migrate towards the node. In this way, the particles are separated. Separation devices can operate in batch [6] or continuous mode [7], and can have single [8] or multiple entrances & exits [9, 10]. Apart from separation, such devices have also been used for particle positioning/manipulation [11, 12], cell detection [13–15], medium switching [16, 17] etc.

The disadvantage of microfluidic devices is the low throughput owing to lower flow rates. When scaled up to the cm scale & millifluidic range ($\dot{Vol} \sim ml\,min^{-1}$), operating the device with only a single node would mean employing (kHz) frequency. This would imply a great reduction in the acoustic force. And yet, continuing to operate in the ultrasonic range would result in multiple nodes, which would eventually concentrate all the particles. While this operation can be used in sedimentation techniques (known as Ultrasonically Enhanced Sedimentation) to remove all particles from the system [18], it does not have the ability to selectively separate them. A more promising method of separation using multiple nodes is using DAF.

DAF can be achieved through different means, the most popular means are by varying the frequency of the source(s). In such DAFs, the nodes move in space and separation is based on the particles' ability to follow this movement. This nodal movement is achieved either by: frequency ramping in a transducer-reflection configuration - by allowing transducer to periodically ramp within a frequency range [1, 2], or by providing a fixed frequency difference in a transducer-transducer configuration in frequency modulation devices [4]. Phase modulation though employing phase difference rather than

frequency, produces nodal patterns similar to that of frequency modulation [3, 19] and is also a suitable means of creating DAF.

Size selective continuous separation of particles using DAF can be achieved by fine tuning the acoustic field and flow parameters to achieve a nodal movement that traps one set of particles (usually the larger sized ones) and separates it as the flow progresses. Though much effort has gone into study of smaller sized particles (~ 10 μm), there is still research needed to be done on separation of larger sizes, the future applications of which could also be large-scale separation of micro-plastics and other contaminants.

1.2. OUTLINE OF THESIS

The thesis aims at studying the behaviour of two novel DAF separation devices, under the influence of different operating parameters. The success indicator of the study is the threshold size of separation. The suspension to be separated contains polyethylene particles of a continuous size distribution between 32-106 μm. The two devices use different DAF mechanisms; one uses frequency sweeping and the other uses frequency modulation. The two devices will hereafter be referred to as the frequency sweep device & the dual frequency device respectively.

The roadmap to studying each device was proposed as follows: First the capabilities & limitations of both device & setup will be studied, and suitable parameters (and their values) such might selectively separate particles will be selected. A Design of Experiments (DOE) will then be designed with the chosen parameters. The DOE will be carried out for both simulations and experiments. The results will then be analysed to correlate the selected parameters with the separation size.

1.3. OUTLINE OF REPORT

In this report, the theory behind acoustic separation is first introduced in Chapter 2. Chapter 3 contains a concise review of existing literature on DAF devices, followed by the formulation of the research scope for the current study. In Chapter 4, a detailed description of the device and the setup is provided, along with the motivations for parameter selection. The 2D COMSOL models are explained thereafter. Chapter 5 contain the results for Device 1 and Device 2 respectively, followed by conclusions and recommendations in Chapter 6. Additional details can be found in the Appendix.

2

THEORY

Acoustic waves are mechanical waves i.e. they require a medium in which to propagate. An acoustic wave can be created by a source of disturbance such as a vibrating membrane; this disturbance is then transferred to the medium via contact with the adjacent medium particles. The wave propagates through the medium by the vibration of the medium particles, creating regions of compression and rarefaction in the medium, and are thus described as 'traveling waves'. The compression and rarefaction lead to local pressure and density changes in the medium. An acoustic wave is thus best described by a measurable property such as variation of pressure. For a wave traveling along the positive x direction, variation in pressure can be modelled as:

$$P = P_0 \cos(\omega t - kx) \tag{2.1}$$

where P_0 is the amplitude of pressure variation.
The usual wave properties apply and are briefly stated below:
ω is the angular frequency, derived from the frequency of the wave f, as $\omega = 2\pi f$
k is the wavenumber, derived from the wavelength λ, as $k = \frac{2\pi}{\lambda}$
c_w is the velocity of the wave in the medium.
The wavenumber and angular frequency are related as $c = \frac{\omega}{k}$

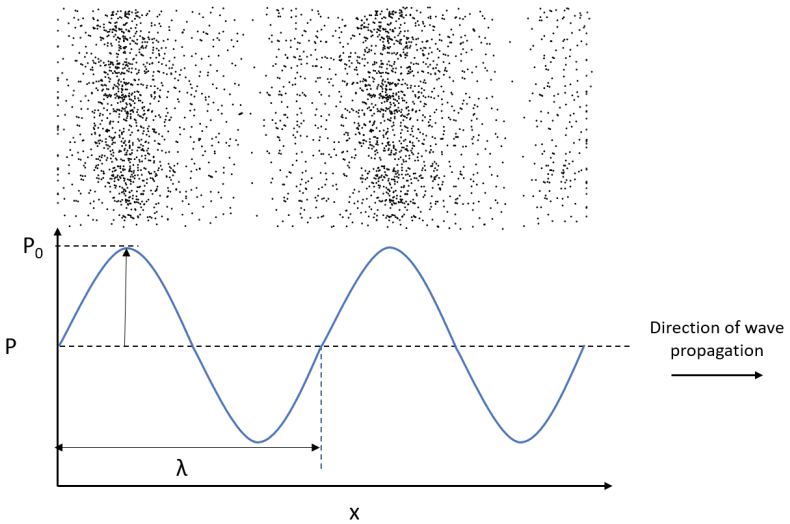

Figure 2.1: Spatial Representation of an acoustic wave traveling in a medium. The medium can be seen undergoing compression and rarefaction, with positive and negative pressure amplitudes attained at regions of maximum and minimum local densities respectively.

An important characteristic of the medium is that of acoustic impedance (Z). Acoustic impedance is the product of the density & speed of sound and is the resistance offered by the medium towards propagation of acoustic waves. It is also the ratio of the acoustic pressure to the acoustic velocity i.e. velocity of medium particles. The acoustic velocity and pressure variation are related as follows:

$$Z = \rho_w c_w = p/v \tag{2.2}$$

2.0.1. STANDING WAVES/STATIC FIELD

When a travelling wave encounters an interface, three modes of energy transfer can occur: reflection, absorption and transmission. Of the three, focus here is on reflection. When the interface is hard (i.e. of acoustic impedance very high in comparison to the medium), as is the case with acoustophoretic devices, the wave is reflected and travels in the opposite direction as the source. The source and reflected wave interact to create a standing wave that oscillates in time, with the wave profile remaining stationary in space. Standing waves can also be produced by two sources placed opposite to each other and operated at the same frequency.

The pressure variation of standing waves can be formed from the summation of two counter-propagating waves, and are as follows:

$$\begin{aligned} P &= P_0 \cos(\omega t - kx) + P_0 \cos(\omega t + kx) \\ P &= 2P_0 \cos(\omega t) \cos(kx) \end{aligned} \tag{2.3}$$

At locations that are even multiples of quarter wavelength $(2n)\frac{\lambda}{4}$, the pressure is at its amplitude, and the locations are called pressure anti-nodes. At fixed locations that are odd multiples of quarter wavelength $(2n+1)\frac{\lambda}{4}$, the pressure assumes its mean value, and the locations are called pressure nodes.

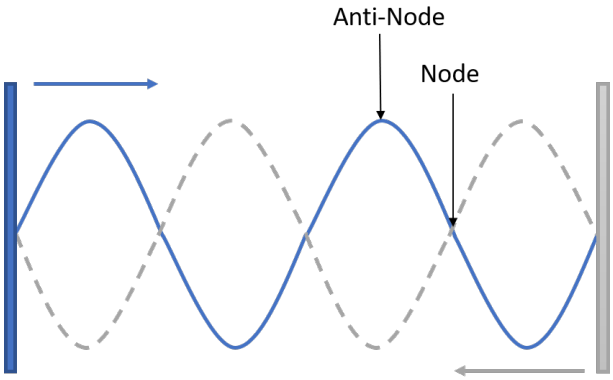

Figure 2.2: Representation of a standing wave. The blue surface represents a source of disturbance. The grey surface can represent either a hard wall or a second source.

2.0.2. DYNAMIC ACOUSTIC FIELD

Unlike a static field where the nodes in the standing wave remain fixed in space, DAF involves nodal movement. Two important mechanisms of creating DAF, as mentioned earlier, are frequency sweeping and frequency modulation.

Frequency sweeping has a transducer-reflector configuration. The transducer excitation frequency is ramped between a fixed frequency range and the ramp is performed periodically, which is known as sweeping. The ramping causes the waveform to be compressed over time causing the nodes to move from transducer to reflector. The nodal speed reduces as the ramp cycle progresses, as the frequency increase causes the nodes to get closer, giving rise to smaller distances and therefore to smaller velocities.
The pressure variation of frequency swept DAF can formulated as follows:

$$P = P_0 \cos\left(\omega(t)t - \frac{\omega(t)}{c_w}x\right) \tag{2.4}$$

At any given time within a sweep period, the location of any given point in the wave pattern, can be described in terms of a fraction n of the wavelength (measured from the reflector end) as:
$x(t) = n\lambda(t)$ At the start of the sweep period, the distance of an arbitrary point from the reflector - x_0 can be expressed as

$$x_0 = n\lambda_0 = n\frac{c_w}{\frac{\omega}{2\pi}} \tag{2.5}$$

After some time t, at an intermediate frequency, the same point has now traveled towards the reflector, and its distance from the reflector can now be described by:

$$x(t) = n\lambda(t) = n\frac{c_w}{(\frac{\omega}{2\pi} + St)} \tag{2.6}$$

where S is the rate of sweep, $S = \frac{\omega_1 - \omega_0}{2\pi T}$
The -ve sign symbolises movement towards the reflector, which is also the reference. The value of n can be found from the relation 2.5 and substituted in relation 2.6, to formulate the distance of the point, at any given time within the sweep period, in terms of its initial position and the sweep excitation provided:

$$x(t) = \frac{x_0\frac{\omega_0}{2\pi}}{(\frac{\omega_0}{2\pi} + St)} \tag{2.7}$$

The velocity of the point at any given time within the sweep period can therefore be found by the time derivative of the above relation:

$$v = -\frac{x_0\frac{\omega_0}{2\pi}S}{(\frac{\omega_0}{2\pi} + St)^2} \tag{2.8}$$

The above concept can be visualised in the below figure, by following the movement of a point in the waveform, in this case the node (the fraction n is 1.5).

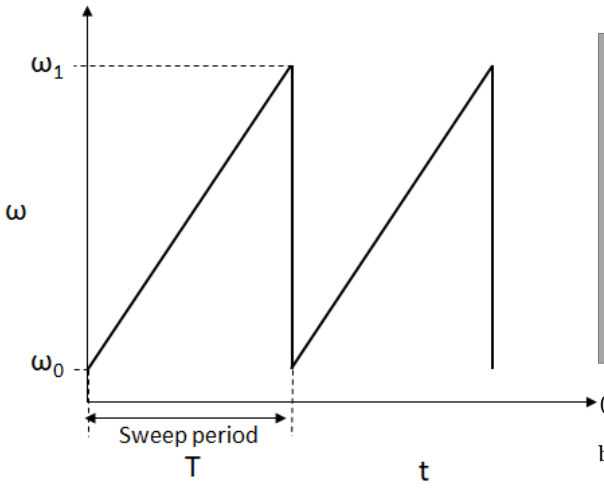

(a) Sweep cycle

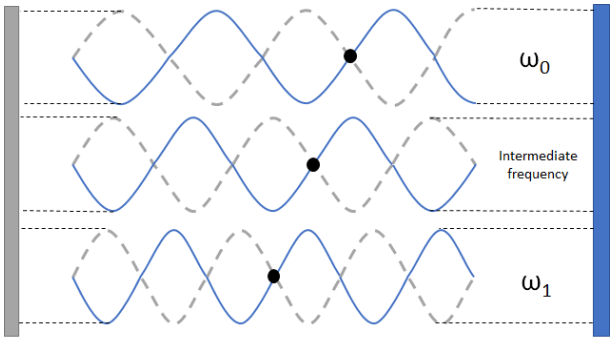

(b) Representation of the movement of nodes (emphasized by a black particle) due to application of a frequency sweep. The blue surface represents a source and the grey surface represents a reflector

Figure 2.3: Frequency sweep

Frequency modulation has a dual transducer configuration; one transducer is excited with a higher frequency (~ Hz) than the other. This difference causes the nodes to move, and the traveling of

the nodes is from the higher frequency source to the lower frequency source. Because of the fixed frequency difference, the nodal velocity is constant. An easier way to represent the two frequencies is by using a central frequency ω_c (average of the two frequencies) and the frequency difference ϵ (applicable only when $\epsilon << \omega_c$).

$$\begin{aligned} \omega_1 &= \omega_2 + \epsilon \\ \omega_c &= \frac{\omega_1 + \omega_2}{2} \end{aligned} \tag{2.9}$$

The pressure variation of frequency modulated DAF (with higher frequency source at the right) can be formulated using the first part of equation 2.10. After substituting relations 2.9 in the first part and reducing the trigonometric identities, the second part of equation 2.10 can be obtained.

$$\begin{aligned} P &= P_0 \cos(\omega_1 t + \frac{\omega_1}{c_w} x) + P_0 \cos(\omega_2 t - \frac{\omega_2}{c_w} x) \\ P &= 2P_0 \cos(\frac{\omega_c}{c_w} x - \frac{\epsilon}{2} t) \cos(\frac{\epsilon}{2c_w} x - \omega_c t) \end{aligned} \tag{2.10}$$

The nodal speed is given as [20]:

$$v = \frac{\epsilon}{2\omega_c} c_w \tag{2.11}$$

2.1. ACOUSTIC RADIATION FORCE

When an acoustic field is applied to a suspension, the suspended particles experience hydrodynamic forces from the surrounding fluid. This force is known as the Acoustic Radiation Force (F_{ac}). F_{ac} acting on a rigid sphere by a 1D plane standing wave, was derived by Gor'kov[21]:

$$F_{ac}(x) = 4\pi r_p^3 k \phi(\rho, c) E_{ac} \sin(2kx) \tag{2.12}$$

F_{ac} causes particles having a positive acoustic contrast factor (ϕ) to move towards the pressure nodes, and are trapped there. If the fluid is in motion, the trapped particles travel along the nodal plane. Similarly particles with a negative contrast factor move towards the pressure anti-nodes and can be trapped there. Greater acoustic pressure amplitude would imply greater acoustic energy density E_{ac} and hence greater F_{ac}. Of note in the above equation, are the particle size (r_p) and wavenumber dependencies of F_{ac}. Larger particle sizes and a higher wavenumber (or higher frequency) of the applied acoustic field imply higher F_{ac} acting on the particle. The above points form the basis for separation devices.

From equations 2.1 and 2.12, it is evident that the acoustic force is period doubled and phase shifted relative to pressure variation. This is represented in Fig. 2.4.

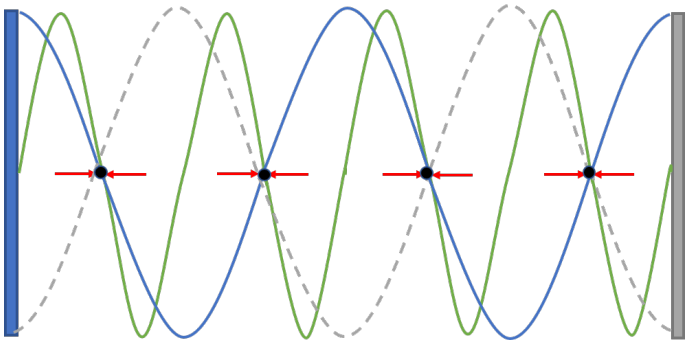

Figure 2.4: Representative waveforms for standing wave and acoustic radiation force. The waveform in blue-grey represents the standing wave with the black circles representing the nodes. The waveform in green represents the acoustic radiation force. The arrows in red indicate the direction in which the force acts for particles with positive contrast factor.

2.2. DRAG FORCE

The movement of the suspension particles in the flow field induces an opposing drag force. The drag force formulation used is based on the flow Reynolds number (Re). Re is calculated from the channel dimensions and flow rate as $Re = \frac{\rho_w u_w D_w}{\mu_h}$.

In the present study, the chosen channel flow rate leads to a Reynolds number ≈ 20 and the flow is laminar. The drag is thus inertial, the formulation for which is given below.

$$F_d = C_d(Re_p).\frac{\pi}{4}d_p^2.\frac{1}{2}\rho_w u_r^2 \tag{2.13}$$

While it is established that the drag is inertial, in this study, the drag correlation used is of significance only while modeling the system in COMSOL to calculate particle trajectories. Here, the inbuilt inertial drag correlation, as proposed by Schiller-Naumann was used:

$$C_d = \frac{24}{Re_p}\left(1 + 0.15Re_p^{0.687}\right) \qquad 1 \le Re \le 800 \tag{2.14}$$

where Re_p is the particle Reynold's number, derived as $Re_p = \frac{\rho_w d_p |u_r|}{\mu_w}$, $|U_r|$ being the absolute relative velocity.

2.3. EQUATION OF MOTION

In most continuous flow acoustophoretic separation devices, F_{ac} and F_d act perpendicular to each other, and the resultant is in the direction of the sum of their vectors. The equation of motion (EOM) can thus be expressed as the sum of the two forces

$$F_{resultant} = m_p a = F_d + F_{ac} \tag{2.15}$$

$$\left(\frac{4}{3}\pi r^3\right)\frac{d^2y}{dt^2} = C_d.\frac{\pi}{4}d_p^2.\frac{1}{2}\rho_w\left(\frac{dy}{dt} - u_w\right)^2 + 4\pi r_p^3 k\phi\left(\frac{P_0^2}{4\rho_w c_w^2}\right)sin(2ky) \tag{2.16}$$

When considering the EOM for DAF, the same formulation 2.16 can be used, except the acoustic field parameters in the equation i.e. k & P_0 need to be replaced with their time-variant counterpart $k(t)$ & $P_0(t)$. The EOM is a second-order, non-linear ordinary differential equation, that can be solved numerically to obtain particle positions and ultimately, their trajectories. In this study COMSOL Multiphysics® Version 5.5 was used to solve the EOM.

The interplay between both forces decides if the particles can follow the nodal movement in DAF. In the absence of an acoustic field, particles follow the streamlines owing to drag. When in the presence of an acoustic field therefore, particle trajectory is based on the direction of the resultant force. Size-based selectivity can thus be brought about in DAF devices, by tweaking the flow and acoustic field parameters such that one group of particles experience greater acoustic force, migrate across the channel and separate out at one exit, while the other group of particles experience greater drag and follow the streamlines to separate out at a different exit.

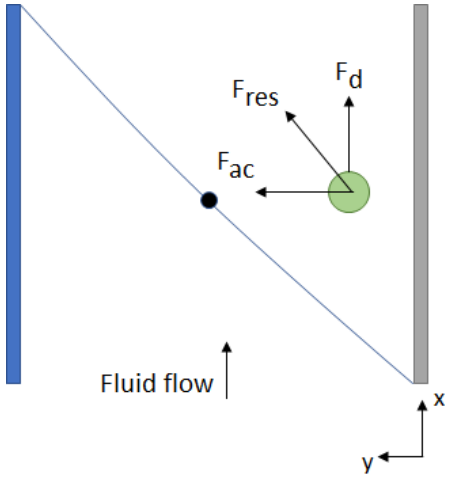

Figure 2.5: Representation of a particle in an acoustic field, in a flowing fluid. The acoustic field has a single node in the middle of the channel (represented by the black circle).

For a given flow field, it was observed during trial experiments that when the DAF is created by frequency sweep, at too small sweep periods, none of the particles can follow the nodes while at too large sweep periods, both large & small particles can follow the nodes. This could perhaps be explained from equation 2.8; larger sweep period would imply slower nodal speeds (across the sweep period), which could mean a greater tendency for the smaller particles to follow the nodes. When the DAF is created by applying a frequency difference, at too small frequency differences, both larger and smaller particles can follow the nodes while at too large frequency differences, none can. This too can be reasoned from equation 2.11; smaller frequency differences would imply slower nodal speed, and hence a greater tendency for small particles to follow the nodes. Selectivity for both cases can then be obtained by applying an intermediate value such that only the bigger particles can follow the nodes. This is generally found by trial simulations & experiments.

3

LITERATURE REVIEW & RESEARCH SCOPE

In this chapter, a few DAF devices that are relevant to the current study have been summarized. Salient points pertaining to operating parameters, mainly the flow rates, applied voltage, size and concentration of particles have been highlighted along with the results.

3.1. FREQUENCY SWEEP

Ebbesen et al. [1] demonstrated separation of 3 & 10 µm polystyrene particles (in water). The main intention was to use the device to separate red blood cells and plasma from blood samples, but the characterization of the device was first done with the polystyrene particles. The device used had two inlets and exits, with the suspension and sheath pumped in individually and the separated particles collected at their respective exits, refer Fig. 3.1.

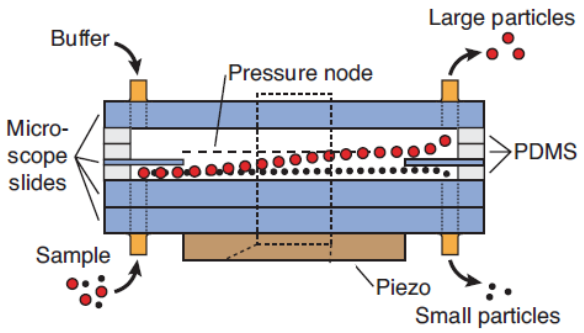

Figure 3.1: Device configuration used by Ebbsen et al. [1]

The study tried to obtain high throughput of particles for a total inlet flow rate of 1 L/hour. High throughput requires larger input flow rates which strengthens the drag force. This requires higher voltage to be applied to the acoustic field to increase the acoustic force. Higher voltage causes heating effects; resonant frequency shifts due to change in density of the medium. The voltage applied to the transducer was also varied upto 55 V_{pp} to find the optimum value for selectivity, which was found to be around 15 V_{pp} for the given particle sizes. Separation efficiency increased when the frequency was linearly ramped as $\pm$ 10 Hz around 899 kHz in 1 ms time periods. Though frequency sweeping was used to demonstrate improved separation efficiency, the effect of different sweep periods on the separation was not demonstrated.

Lipkens et al. [2] studied the effect of sweep period and frequency range on particle trajectories and velocities. The particles were 6 µm polystyrene suspended in water. The device was cross-shaped, with a single inlet-exit located South-North for the suspension to flow through, and the acoustic field

located West-East. The flow and acoustic field interact at the square-region in the center. The particles were harvested from the East-end of the cross, refer Fig. 3.2a.

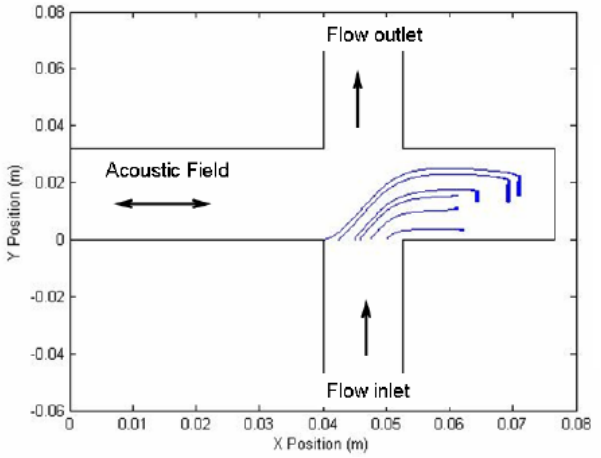

(a) Device configuration used by Lipkens et al.

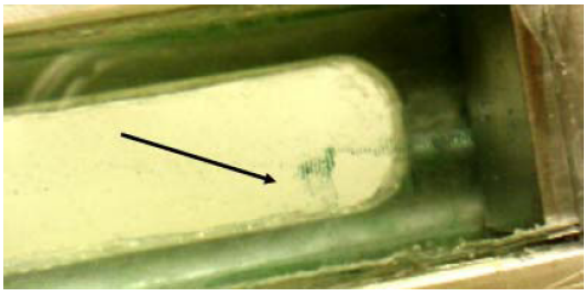

(b) Photo of the East-end of the resonator at 237s, where particles are seen to be agglomerating

Figure 3.2: Separation of 6 µm particles from water, Lipkens et al. [2]

Frequency was linearly ramped for 9 cases; combinations of ±20, ±40, ±100 kHz around 1.89 MHz frequency, 40 V_{pp} and for 1 s, 0.5 s, 0.25 s sweep periods. A numerical study was conducted along with experimental validation. Good agreement was found for the theoretical and experimental velocities. The velocities were found to be proportional to swept frequency range and inversely proportional to sweep period. The study also states that the flow rates were varied between 30-250 ml min^{-1}, but there were no other mentions on the effect of these flow rates. Experiments showed separation of the particles from the medium, by concentrating them at a nodal location. The particles coalesce to form a large lump, when exposed to the acoustic field for a long time. When heavy enough, these agglomerates sink to the bottom of the channel, refer Fig. 3.2b. Here as well, frequency sweeping was used to demonstrate varying particle velocities at different time periods, but the effect on the frequency range and sweep periods were not demonstrated.

3.2. PHASE MODULATION

Simon et al. [3] demonstrated separation of 10 & 15 µm polystyrene particles (in water) with phase modulation. The device was asymmetric with 3 inlets and 2 exits. Of the 3 inlets, 2 are for the medium flow (referred to as sheath flow) and 1 is for the particle flow; all 3 are of different sizes. The flow rates were kept constant for the duration of the experiment; 0.45 µl min^{-1}, 2.5 µl min^{-1} for the smaller and larger sheath flows respectively, and 0.2 µl min^{-1} for the sample flow. The cycle consisted of a ramp time where the phase was shifted gradually from 0° to 360°, followed by a rest time where the standing wave field is simply static. The operating frequency was 12.6 MHz at 23 V_{pp} input voltage. Ramp times between 0.6-1 s were tested, to find out which one yielded selectivity. At larger ramp times both particles could follow the nodal pattern, while at smaller ramp times neither could. Optimum selectivity was found at a ramp time of 0.7 s, when the larger particles could follow the nodal pattern, while the smaller ones could not. Rest time was provided to establish equilibrium; the larger particles settled into the next node position, while the smaller ones remained at the initial one, refer Fig. 3.3. 100% efficiency of the target (large) particles was found at one exit while 94.5% efficiency of the waste (small) particles was found at the other exit.

A similar study was performed by Skotis et al. [19]. Here the interplay between rate of phase modulation and the resting time forms the core of the separation process. Polystyrene particles of size 6, 10, 45 µm (in water) were tested for different ramp and rest times and the optimum values were recorded. These were then used to test for selectivity in a mixture of 1) 6 & 10 µm 2) 10 & 45 µm. The operating frequency was 4 MHz, the flow rates were not specified. A parametric study was carried out with the ramp and rest times, with tests leading to purity >90% being considered successful. Ramp time was found to be more influential than the rest time. The purity and efficiency of separation for

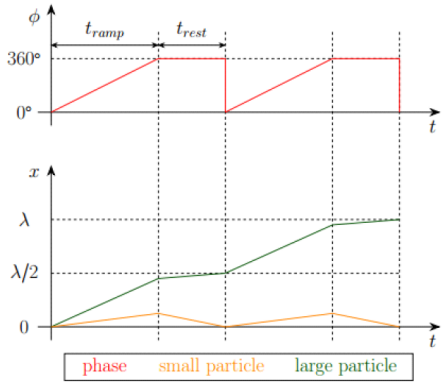

Figure 3.3: Ramp and rest cycle showing the movement of particles at different points in the cycle, Simon et al. [3]

each test was found by simulation and then experimentally validated. For the first mixture, a maximum of ≈97% purity and efficiency was found at ramp and rest times of 15 s, while the second mixture had a maximum of ≈100% purity and efficiency at ramp time of 8 s and rest time of 4 s. There seems to be good agreement between the theoretical and experimental values.

3.3. FREQUENCY MODULATION

A method for separation using frequency modulation was demonstrated by Simon et al. [4]. The device used a dual transducer configuration, and was asymmetric with 3 inlets of different sizes (2 sheath and 1 sample) and 2 exits, refer Fig. 3.4a. The particles to be separated were 5-14.5 µm polystyrene particles, dispersed in water. Groups of 5,6 µm, 6,8 µm and 10,14.5 µm were tested.

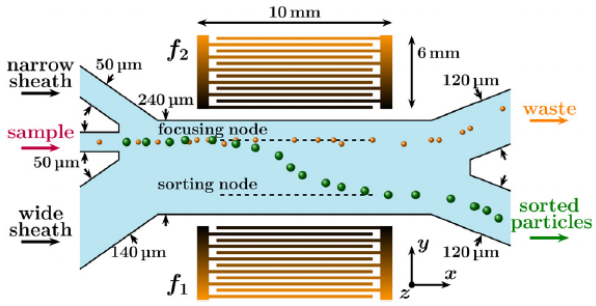

(a) Device configuration used

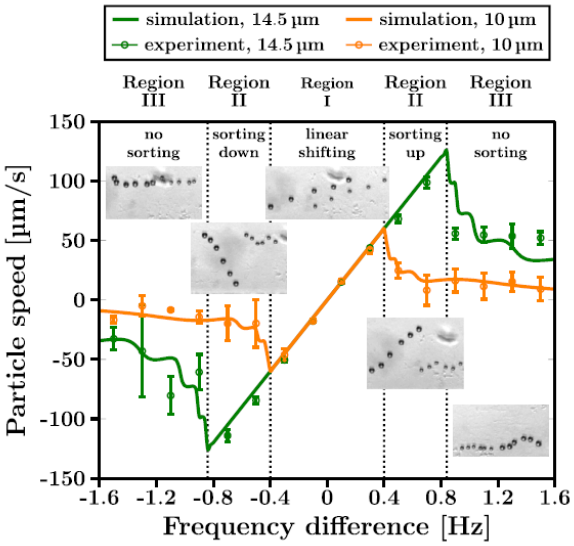

(b) Theoretical and experimental average particle speeds at different frequency differences for 10,14.5µm particles.

Figure 3.4: Size based separation of 5-14.5 µm particles, Simon et al. [4]

The study also show bi-directional sorting in which target particles can be made to flow through either of the exits. Similar to the ramp and rest cyles of before, the method uses frequency modulation for the first half of the cycle. The larger particle follows the nodal pattern closely, while the small particle lags behind. The next half cycle is for the particles to come to equilibrium. The small particles relax into the initial node while the big particles relax into the next node, forming the basis of selectivity.

The central excitation frequency was 13.3 MHz. Bidirectional sorting was exhibited when changing the direction of the higher frequency excitation and by varying the ratio of the two sheath flows, refer Fig. 3.4a. The frequency difference needed for sorting was found by applying a range (±1.6 Hz) of frequency differences and choosing two ranges (-0.8 to -0.4 Hz, 0.4 to 0.8 Hz) in which the particles showed separation.
A sensitivity analysis for flow was also conducted by varying the inlet flow rates to find purity and efficiency. It was found that for a given size ratio, the two bi-directional sorting scenarios - varying frequency difference, varying flow rates - were equivalent. Voltage applied to the transducer was also varied to check the effects on purity and efficiency. Scenarios were classified as sorting when both purity and efficiency were >90% and non-sorting when <70%. An exercise was also carried out to find out the size ratio (larger to smaller particle) threshold below which the purity and efficiency of separation drops lower than 70%, and was found to be ≈1.2.

3.4. SIZED BASED SEPARATION IN OTHER DEVICES

There was not much literature that could explain size based separation in acoustic devices. Hence literature pertaining to other devices were also studied to try and find common concepts to be implemented in the current study. A device similar in purpose, but using a different separating mechanism was found and has been summarized briefly below.
The concept of size based separation was explored by Fuh, Myers & Giddings in [22] in their proposed concept ”Analytical SPLITT Fractionation (ASF)”. A SPLITT or Split thin flow fractionation device usually consists of a channel <0.5 mm, with two inlets (one for the medium and one for the particles) and two exits, each inlet and outlet pair separated by thin splitter plates. Separation happens across the channels where the field is applied. The field could be any: gravity,magnetic,electric etc., with larger particles that are greatly affected by the field migrating across the channel and separating out from the inlet stream. In SPLITT devices the medium inlet flow rate is usually set higher than the particle inlet flow rate. This helps compress the particle stream into a thin layer, encouraging better separation resolution.

ASF is a SPLITT device, which can work on a continuous stream of particles and divide them into two groups based on a cutoff size. An example application of the ASF device could be production of particles, particle size characterization, and cleanup of particulate matter from which ”oversized particles” need to be removed. The study was both theoretical and experimental. A cutoff size for these oversized particles was proposed; the size was calculated using the volumetric flow rates, strength of the field and channel dimensions. Here the field studied was gravity. Flow rates being easier to manipulate were favoured to find different cutoff sizes in the study. First, the inlet flow rates were found by finding a trade-off between having a thin particle inlet stream, and avoiding unwanted dilution of the outputs. For given inlet flow rates, the outlet flow rates were then varied for different cutoff diameters. The theoretical cutoff diameters were also experimentally validated and were found to be in good agreement.

3.5. RESEARCH SCOPE

From the review of literature on DAF devices, it was found that most separation studies were limited to a set of two to three distinct particle sizes, for which optimum separation conditions were found such that each size exited through separate outlets. The particles were also mostly limited to sizes of ≈10 µm. Not a lot of research has been done on larger sized particle separation and on a larger scale. The current study aims to fill this gap by evaluating two DAF devices to find if they are capable of separating particles of a wide range, between 32-106 µm, while operating at a high throughput of 1000 ml h^{-1}. The study wants to find if, by varying the operating parameters in the device, different size distributions can be obtained; if say distributions between 32-50, 50-106 µm or 32-80, 80-106 µm etc. can be obtained using the same device, just by applying different conditions. In order to evaluate this, the study aims to find the relation between different operating conditions and cutoff size or threshold size at which separation occurs.

Therefore, the research objective is formulated as follows:

> To study the effects of operating parameters on the threshold size for frequency-modulated and frequency-swept dynamic acoustic field separation devices, by means of a design of experiments that includes numerical prediction of the threshold size and experimental validation of the same.

In this context, the research questions are then framed as follows:

1. What are all the factors in the setup and in the device, that could influence the threshold size of separation?
2. How do the selected factors correlate to the threshold size?

4

MATERIALS & METHODS

4.1. DESIGN OF EXPERIMENTS

In order to study the separation ability of each device, it was first proposed that a Design of Experiments (DOE) be made. The parameters to be studied can be classified into 3 groups:

1. **Geometric:** 1. Multiple inlets & exits 2. Positions of Inlet & exit guideways 3. Angles of Inlet & exit guideways
2. **Acoustic:** 1. Pressure Amplitude 2. Sweep period/frequency difference
3. **Flow:** Inlet & exit flow rates

During initial trial experiments, geometric features of the device were eliminated, as they would increase the parameters to be monitored and complicate the model. It was then decided that the study would be made on only one geometric design where the inlet and exit dimensions are equal, and the design is symmetric about all mid planes. In order to create a DOE where the parameters could be easily measured, and where the DOE validation can be satisfactorily completed in the time scale of the thesis, the following were decided upon:

1. 3 different parameters were proposed as the factors of the DOE: 1. Inlet Flow Rate 2. Exit Flow Rates 3. Sweep periods/frequency difference.
2. For each factor, 3 different values can be chosen, so that the total number of experiments comes out to be $3^3 = 27$.
3. Each value needs to be evenly spaced so that interpretation is easier and a wider range is covered.

The DOE was created in Minitab 18. A General Full Factorial design was created with 3 factors and 3 levels. The factors provided were 1. Particle inlet flow rate (Particle Inlet V1), 2. Reflector exit flow rate (Reflector Exit V4), 3. Sweep Period / Frequency Difference. As the flow rates at inlet and exit are complementary (i.e. sum = 1000 ml h^{-1}), it was easy to implement the DOE in this manner. The results to be analysed were the threshold sizes from simulations and experiments.

The analysis of the DOE was done using the factorial analysis available in Minitab. There are 3 main charts obtained from the analysis: the Pareto chart of standardized effects, the Main effects chart & the Interaction effects chart. In general, a Pareto chart is used in statistics, to identify the frequency of a defect/loss and find out the main causal factors. It is based on the principle that 80% of the effects come from 20% of the causes. In a DOE as well, the Pareto chart is useful to identify the main factors that influence the result. For a given confidence interval Minitab calculates the effects of each factor, as well as a critical effects value. Factors whose effects exceed the critical value are deemed significant. The Pareto chart however only compares absolute values of the effects to find their

significance, and cannot describe if they increase or decrease the response. This can be viewed in the main effects chart & the interaction effects chart. Main effects are the effects of each independent factor on the threshold size. The interaction effects describes how the effect of one independent factor influences the effect of another when defining a threshold size. In this study, a 95% confidence interval was chosen, along with backward elimination for a stepwise factorial analysis. In backward elimination, the analysis is performed in stages; it begins with all factors included in the model. The pareto analysis is performed and the insignificant factors are removed in each stage, with the analysis ending only when all the factors are significant.

4.2. EXPERIMENTS

4.2.1. SETUP

An overview of the setup is given in Fig. 4.1. A detailed explanation for each component is given in the subsequent sections

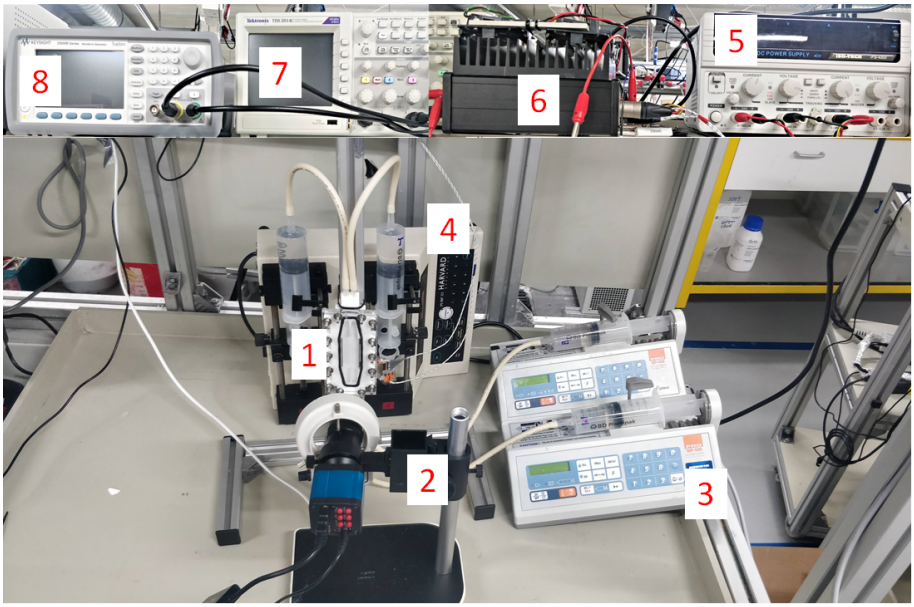

Figure 4.1: View of the Setup
Annotations: 1.Device 2.Microscope Camera 3.Inlet Pump 4.Exit Pump
5.DC Power Supply 6.Amplifier 7.Oscilloscope 8.Dual-Waveform Generator

4.2.2. DEVICE

4.2.2.1. CONSTRUCTION

The two devices under study have a common layout for separation; each of them have two inlets and outlets. Of the two inlets, through one flows the suspension of particles and through the other flows the carrier medium (water). The two flows emerging from each inlet, merge into a single channel flow that passes through the acoustic chamber. Separation of the particles occurs in this chamber, and separated particles then exit from the two outlets. The devices were oriented vertically such that the flow is against gravity. This configuration was chosen for its convenience in handling the prototype. A schematic representation of both devices can be seen in Figs. 4.2 & 4.3. The actual devices are given in Figs. 4.4,4.5.

The devices' dimensions were restricted by the size of the transducer. The transducer measures 50x10x1 mm. The lengths and heights of the acoustic chambers were defined by these dimensions. The widths of the chambers were dependent on the number of nodes required to have a multi-nodal field, without compromising on the field strength. The widths for both devices were thus 20 mm. Existing designs for the device were modified to ensure smooth expansion of flows at the entrance and exit of the device. To enable this a circular-square draft was provided at the entrance to the device.

Also, the guideways separating the two inlets and outlets were angled at ≈8° for the frequency sweep device, ≈12° for the dual frequency device respectively.

1. **FREQUENCY SWEEP DEVICE:** The reflector was of the same dimensions as the transducer and was made of stainless steel. A schematic representation of the device is given in Fig. 4.2.the transducer-reflector facing each other, calculating the dimensions of the acoustic chamber is straightforward; the chamber is thus chosen to be 50x20x10 mm. The inlet and outlet flow dimensions were then chosen to be 25 mm each. Care was taken to see that the guideways stop exactly at the entrance and exit to the acoustic chamber so that the particle separation occurs only in the chamber.

Figure 4.2: Schematic representation of the Frequency Sweep Device
Annotations: T-Transducer R-Reflector
The white space indicates the regions where the fluid would flow.
The area enclosed by the dashed green lines is the acoustic chamber

2. **DUAL FREQUENCY DEVICE:** In contrast to existing frequency modulation devices, the DAF was created by means of two transducers placed perpendicular to each other. Effects of reflection would normally be present if the transducers were placed opposing each other. This was seen in the research conducted by Beelen & Kandemir [20]. It was therefore expected that this geometry helps avoid reflections in the acoustic field. It follows that when the acoustic field generated at each transducer source is resolved in space, only the vertical components of the acoustic field act to create the standing waves. The horizontal components of both fields remain as traveling waves. Their resultant acoustic radiation force is negligible in comparison to the forces from the standing waves, and ideally can be ignored.
   The perpendicular orientation of the transducers coupled with the need for a straight channel flow in the device, implied there was a requirement for walls that allow straight flow inside while simultaneously transferring the excitation from the transducers. This was done by means of acoustic windows. The acoustic windows were made of polyurethane. Before attaching to the device, the window was pre-tensed to prevent sagging when the fluid is filled, and the ends were affixed to the wall with glue. It was also proven that the acoustic windows do not interfere with the acoustic field and merely transfer [20]. The guideway lengths here are restricted by the positioning of the transducers.

For ease of use, the terms ”Transducer” and ”Reflector” will also be used for the dual frequency device; they refer to the higher frequency source and the lower frequency source respectively.
When describing the input conditions hereon, the following notation is used:
$\dot{V}_1$ - $\dot{V}_2$ - $\dot{V}_3$ - $\dot{V}_4$ (ml h^{-1}) - sweep period/frequency difference (s/Hz)

4.2.2.2. FABRICATION

Both prototypes were designed using KeyCreator software and 3D-printed using Polylactic acid (PLA) material. The circle-square draft is constructed with a support structure made of Polyvinyl alcohol (PVA), to prevent warping. Once the device was printed, it was immersed in water to let the PVA dissolve. Ultimaker S5 was used for the 3D printing.

The prototypes were enclosed by a Poly(methyl methacrylate) (PMMA) cover, to enable visualization of the particle movement. The upper surface of the prototypes had grooves encircling the main flow

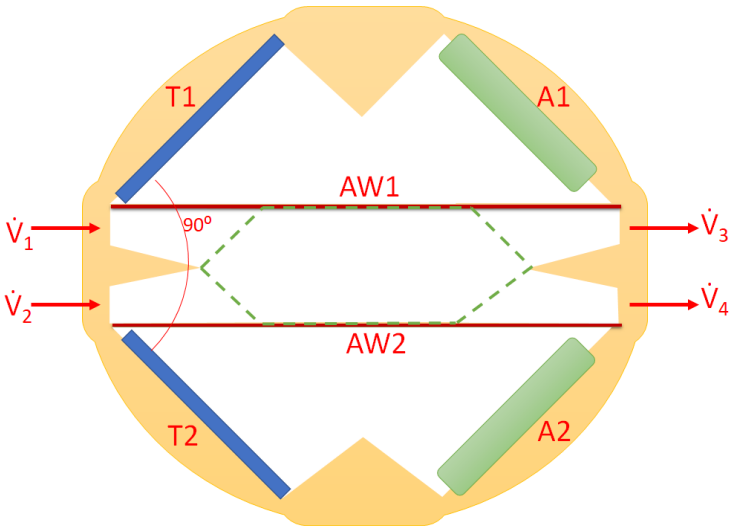

Figure 4.3: Schematic representation of the Dual Frequency Device
Annotations: T-Transducer A-Absorbent block AW-Acoustic Window
The white space between the Acoustic window indicate the regions where the fluid would flow, the spaces on either side are dead volumes where the fluid merely propagates the acoustic field. The area enclosed by the dashed green lines is the acoustic chamber

area. A rubber gasket was affixed with glue in the groove; the PMMA cover was then attached on top of the 3D printed prototype by means of screws, with the gasket enabling the prototype to be leak-proof.

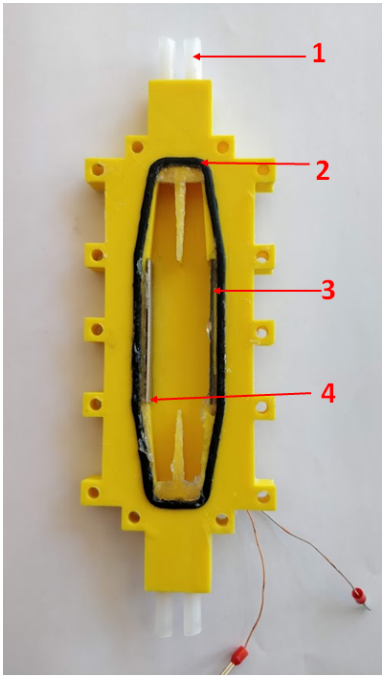

(a) Annotations: 1.Tubing 2.Rubber Gasket 3.Transducer 4.Reflector

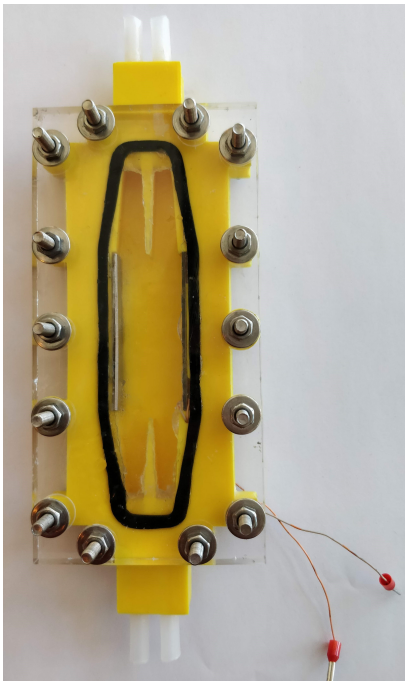

(b) Device with PMMA cover attached on top

Figure 4.4: Frequency Sweep Device

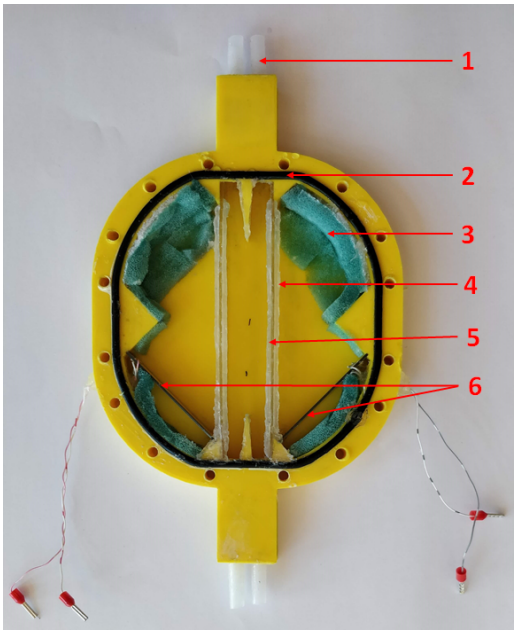

(a) Annotations: 1.Tubing 2.Rubber Gasket 3.Sponge 4.Silicone Gasket 5. Acoustic Window 6. Transducer

(b) Device with PMMA cover attached on top

Figure 4.5: Dual Frequency Device

In both prototypes, the upper surfaces of the guideways were painted with silicone to prevent mixing of the flow streams. Holes were present in the prototypes to allow the transducer wires to pass through. Once the transducers were put in place, the holes were filled in with silicone. Additionally, in the dual frequency prototype, silicone 'gaskets' were made by painting silicone layers on the upper and lower surfaces of the acoustic window, such that the flow was contained within the acoustic chamber. Short pieces of Polyethylene LDPE tubing of 6 mm outer diameter were attached to the inlet and outlet holes. Additionally Ecolab kitchen sponges pieces were stuck opposite & behind the transducers, to avoid reflections from the device.
At the start of every experiment run, the prototypes were washed thoroughly to get rid of particles stuck to the walls, and then filled with water. Care was taken to minimise the occurrence of air bubbles and leakages in the system, as a loss of pressure would affect the flow field.

4.2.3. FLOW FIELD

For both inlets and outlets, 100 mL syringes act as the source and collection units. Two syringe pumps - Aitecs PRO SP-12S were used to provide inlet flows. Harvard Apparatus Dual Syringe Pump 33 was used for the exit flows. The syringes were refilled/emptied during every experiment run. Masterflex Norprene A-60-F tubings of inner diameter 6.4 mm mm were used to provide connections between the prototype and syringes.

4.2.4. VISUALIZATION

Eakins 680520 14 MP microscope camera was used to visualize the flow. Videos of the flow were captured and particle trajectories were obtained by forming stacks of the videos using FIJI ImageJ software.

4.2.5. ACOUSTIC FIELD

4.2.5.1. EXCITATION

Noliac NCE41 piezoelectric transducers were used to create the acoustic field. Since the transducers remain in contact with water throughout, short circuiting was prevented by applying a coat of polyurethane lacquer to the transducer surface, and letting it dry before usage. The waveform and sweep profile of excitation to the transducers were provided by Keysight Trueform 33512B dual

waveform generator. The signal was amplified with a custom-made amplifier. The resultant waveform was monitored on the Tektronix TDS2024C oscilloscope.

4.2.5.2. ADMITTANCE MEASUREMENTS

It is preferred that the transducers be excited at a frequency where, for a given input, the response amplitudes are maximum. This phenomenon is known as resonance, and occurs at frequencies having higher electrical admittance values in comparison to the rest of the range. Admittance of a system - in this case the transducer - is the ease with which current flows through it. Admittance of the transducers were measured using the HP4194A Impedance Analyzer. The measurements were carried out with the transducers placed in the devices and filled with water.
Transducers were sometimes changed in the middle of experiments because of the tendency of the connecting leads to break off from the solder on the transducer. When this happened, the replacement transducers were found such that they had highly similar admittance curves.

Figure 4.6: HP4194A Impedance Analyzer

4.2.5.3. PRESSURE AMPLITUDE MEASUREMENTS

Pressure amplitude of the acoustic field was measured by means of Polytec OFV 5000 laser vibrometer.

SETUP: The instrumentation consists of a sensor head attached to a controller unit. A data acquisition module - Picoscope 3000 Series oscilloscope - transfers the data to a PC. Picoscope 6 software provides the readout.

The transducer was inserted in a PLA fixture which was placed in a glass aquarium filled with water. The sensor head with the laser beam was pointed perpendicular to the transducer surface. The transducer was excited and the resultant vibration velocities were captured.

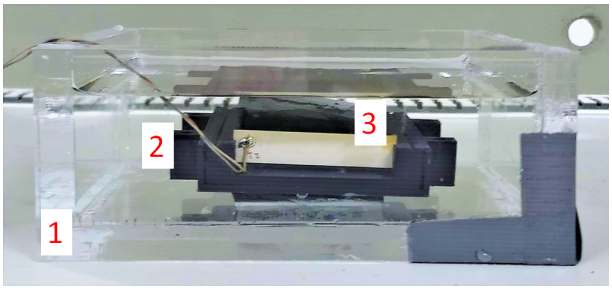

Figure 4.7: 1.Glass Aquarium 2.PLA fixture 3.Transducer

Figure 4.8: Sensor head

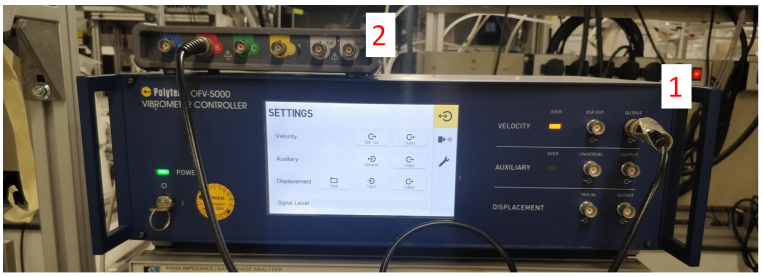

Figure 4.9:
1.Controller 2.Data Acquisition Unit

PRINCIPLE: The vibrometer works on the principles of Doppler effect and interferometry. In essence, the sensor head houses a laser unit from which a single laser beam is split into a test beam and a reference beam. The test beam is focused on a single point on the sample, which reflects it. This reflected beam along with the reference beam fall on the detector. The vibrating sample (in this case, the transducer) introduces a doppler frequency shift owing to its movement. This doppler shift is measured from the interference of the reflected beam with the reference beam, from which the velocity of the vibrating sample is calculated

For both frequency sweep and dual frequency measurements, the same transducer was used in the setup. A long sweep period of 250 s was made in the operating frequency range for both measurements. Only the voltage values at which the transducers were to be operated in the experiments, were set accordingly. Since equal pressure amplitudes were set for the dual frequency transducers, a single pressure amplitude measurement was deemed sufficient.

For each reading, the following software settings were set:

- The spectrum was changed from time to frequency domain and Hanning window was chosen as the smoothing function.
- The measurements to be captured were changed from instantaneous to ”Peak hold” values i.e. the maximum amplitude of velocity that could be captured during the measurement time.
- A fixed measurement time for each reading was not chosen, instead the capture was stopped after the incoming signal steadied and there were no perceptible changes in the amplitude.

The measurements obtained were electrical voltage signals, which were manually converted into velocity by multiplication with a pre-defined conversion factor; in this case 1 V corresponding to a velocity of 200 mm s^{-1}. A set of 5 readings were taken for each device, and the averaged results were used as input for the simulations. For the frequency sweep, the results over the entire frequency range were used, inputted as the variable pressure amplitude function $P_0(t)$. For the dual frequency device, single pressure amplitude value P_0 at the operating frequency was used.

4.2.6. PARTICLES

4.2.6.1. PARTICLE SIZE ANALYZER

At the end of each experiment run, two samples were obtained; one from the transducer outlet and one from the reflector outlet. The Particle Size Distribution (PSD) for each sample was made using DIPA 2000 Analyzer from Donner Technologies. For each sample, DIPA carried out the measurement thrice and presented the average of measurements as the final results.

In order to understand the separation of the given particle range, the concept of threshold size is introduced. As mentioned in the research scope, threshold size is a cutoff size at which the smaller sized distribution exits via the transducer outlet, and the bigger sized distribution exits via the reflector outlet. The separation can then be interpreted as the filtration of particles into two outlets based on the threshold size. Either of the samples can be measured to find the threshold. The threshold is then either the largest size in the transducer distribution or the smallest size in the reflector distribution.

The PSD is presented as a volume histogram of: particle size versus percentage of volume occupied by each size. As mentioned earlier, DIPA needs sufficient particle concentrations to present the results with a satisfactory confidence interval (>95%). This would mean that if there are not enough particles of a sufficient size group, they would not show up in the histogram. This in turn would mean that while measuring transducer outlet samples, a sufficiently long discontinuity in distribution could also be construed as the threshold size, with particle sizes after the break taken as outliers. Therefore, to avoid confusion in choosing a size, a standardized measurement index - the D90 size of the distribution is taken as the threshold size. D90 is the size under which 90% of the distribution falls. In choosing this size, it is therefore acknowledged that transducer outlet sample is 10% 'impure' i.e. it contains atleast 10% overlap with reflector samples. The actual impurity can then be found in the reflector samples, by finding out the overlap of reflector distribution with transducer distribution.

Analogous to D90 size of the transducer distribution, the threshold size can also be identified in the reflector distribution. This would be the D10 size i.e. the size above which 90% of the distribution can be found. The impurity in this case will then be found from the overlap of transducer distribution with respect to reflector distribution.

SETUP: The DIPA 2000 consists of a laser unit with a focused rotating laser beam, incident on a glass chamber in which the sample is circulated through a peristaltic pump (Masterflex L/S Easy Load II).
PRINCIPLE: The particle size measurement is based on the concept of "Laser Obscuration Time", where the diameter of a random particle is calculated as a product of the time for which the laser beam is obstructed by the particle, and the velocity with which the beam rotates.

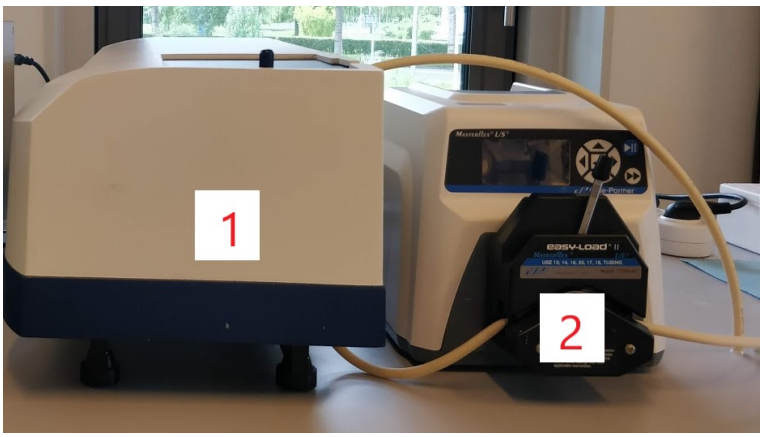

Figure 4.10: DIPA 2000 Particle Size Analyzer
1. Laser Measurement Unit 2. Peristaltic Pump

4.2.6.2. PARTICLE CHARACTERISTICS

The particles used in the study were polyethylene microspheres of diameters ranging between 32-106 µm (Cospheric LLC). The density of polyethylene ($\approx 1\ g\ cm^{-3}$) allows the particles to be neutrally buoyant, so that gravity effects can be ruled out to make things simpler. The particles were of 4 different size distributions within this range, with overlaps in between, thus giving a continuous distribution when mixed. Each size distribution had a different colour for easy visualization.

Suspensions used in the experiments consist of the particles mixed in de-mineralized water with a

small amount of surfactant CTAB, added to prevent agglomeration. The suspension needs to be evenly mixed at all times, so as to obtain the same PSD during every experiment run. The suspension was hence stirred constantly with the help of a magnetic stirrer.

In order to observe the particle size distribution (PSD) in each group, a small amount of each was individually mixed in demi-water and tested in the Particle Size Analyzer. Since it was suspected that surfactant molecules could influence the size distribution, the above exercise was conducted without adding surfactant, as a result of which aggregates could be seen in the sample. The measured PSD was then corrected for the aggregates by eliminating the larger sizes and can be seen in Fig. 4.11. It can also be seen that the suspension is multi-modal, having 4 distinct modes in each size group.

Colour	Diameter Range (µm)	Density ($kg\,m^{-3}$)
Red	32-38	998
Cyan	43-58	1000
Orange	63-75	1006
Blue	90-106	1002

Table 4.1: Microsphere specifications

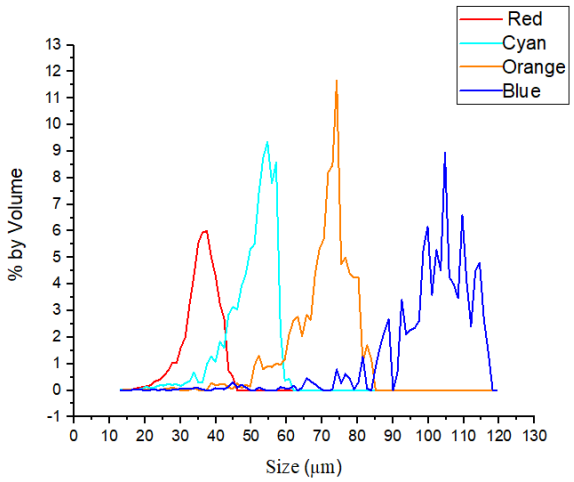

Figure 4.11: Size distribution of Individual Particles

The density and speed of sound properties of polyethylene and water can be used to find the acoustic contrast factor of the particles, which was found to be ≈ 0.085 (c_w = 1481.4,m s^{-1}, c_p=1720 m s^{-1}). The particles thus have a positive acoustic contrast factor and would be trapped at the nodes.

4.2.7. SELECTION OF PARAMETERS

1. **FLOW RATES**

   The net channel flow rate was chosen as 1000 ml h^{-1}; it follows that the sum of flow rates at inlet and exit each need to be 1000 ml h^{-1}. The following points were set as the basis for choosing the flow rates:

   - It was first decided that for the inlet flows, water flow rate should be higher than the particle/suspension flow rate. This follows from the study done by Giddings that when the carrier medium flows at a higher flow rate than the particles, it compresses the particles into a thin layer, which offers better separation resolution.
   - Based on the above, the exit flow rates selected were such that they further enabled the formation of the thin layer.
   - The flow rates chosen should be slow enough not to empty the 100 ml syringes before sufficient amount of separation has occurred; as this leads to poor exit samples that do not have enough particle concentration to give a particle distribution of sufficient confidence interval. It was then decided that a split of 900 - 100 or 800 - 200 ml h^{-1} were not suitable.

2. **OPERATING FREQUENCY**

   For both devices, selection of operating frequency was based on the resonance measurements obtained from the impedance analyzer. Based on these measurements, in the frequency sweep device, the range containing maximum resonant frequencies was identified. In case of the dual frequency device, the lower operating frequency was identified. This is the frequency at which the transducers have the highest but equal admittance values.

   Note: The manufacturer specifications indicate that the transducers have resonance around 2 MHz. We are further interested in the range in which they can be applied, which is why this exercise is carried out.

3. **OPERATING VOLTAGE**

   The operating voltages for each device (found in conjunction with the sweep period/frequency difference) were selected such that they are neither too high that there is sufficiently strong acoustic force for all particles to migrate, nor too low that the acoustic force is not strong enough for even the bigger particles to migrate.

4. **SWEEP PERIOD**

   The values for sweep periods were selected by tweaking the voltage & sweep periods multiple times, and following the particle trajectories with the microscope camera. In some cases when it was not sufficient to distinguish by eye, particle size measurements were also made. The sweep periods were selected such that the large particles separate over the length of the acoustic chamber, and are able to reach the outlet. At too short sweep periods, the larger particles separate immediately at the entrance to the chamber, and migrate across the channel towards the reflector in a short distance. Because of the parabolic profile of the flow, these migrated particles assume a very low velocity and do not reach the exits before the end of the experiment. Similar to the flow rate selection, this leads to poor reflector exit samples that do not have enough particle concentration.

5. **FREQUENCY DIFFERENCE**

   Here as well, the values were selected by tweaking the voltage & frequency difference, and following the particle trajectories with the microscope camera. The same logic of sufficient separation distance was applied.

6. **SUSPENSION CONCENTRATION**

   Different concentrations of the sample were initially tested. Favourable candidates were found to be samples with equal number of particles & sample with equal weights of particles. The final concentration was chosen with the following constraints:

   - There are enough particles of each group for the Particle Size Analyzer to detect with sufficient confidence.
   - Larger particles (orange & blue) had a greater tendency to stick to the channel bottom and sides. There are enough particles to be sufficiently detected even after some are lost.
   - The volume histograms at the two exits can be better interpreted.
   - The concentration is low enough to avoid particle-particle interaction (Ley & Bruus [23]).

4.2.8. LIMITATIONS

Initially it was thought of including purity of the reflector side samples as a performance indicator of the experiments. Purity was then defined as the percentage of the reflector sample having size greater than the threshold size. During trial experiments it was observed that the large particles (orange and blue) had a greater tendency to sink to the bottom than the smaller ones (red and cyan). Even with the careful selection of flow and acoustic field values, under some conditions, these particles were also pushed against the reflector plate, rendering them unable to reach the reflector outlet. This resulted in some loss of the larger particles, which if it were preventable, could have strengthened the reflector side curves in conditions of good separation. Seeing as it is not possible to count the 'lost' particles, it was decided to study only threshold size as the indicator for separation. But it would seem incomplete

to present the results without a purity indicator to judge the separation of the device. Hence a self devised scale of purity has been presented here:
Purity >50% - Good separation,
Purity between 30-50% - Average separation,
Purity <30% - Poor separation

4.3. SIMULATIONS

Available 2D COMSOL models for both devices were used for this study. The models were provided by the author's supervisor H. Kandemir. The models were used after minor modifications done by the author, such as incorporating a 4th particle group which was not previously present, and modifying the drag force formulation. Both models have almost the same configurations, except for their geometry and the acoustic field.
Two separate studies were created. The first study is a stationary study that solves for the Laminar flow field. The second is a time dependent study that solves for the particle trajectories under the influence of the different forces.

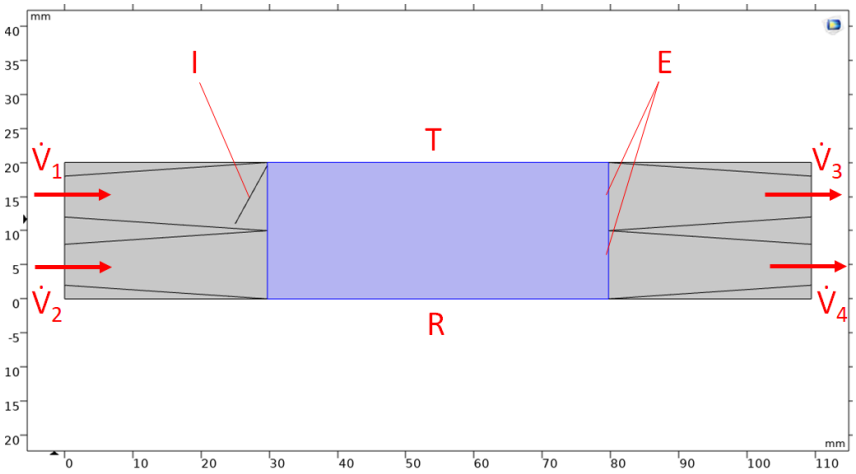

(a) Frequency sweep device

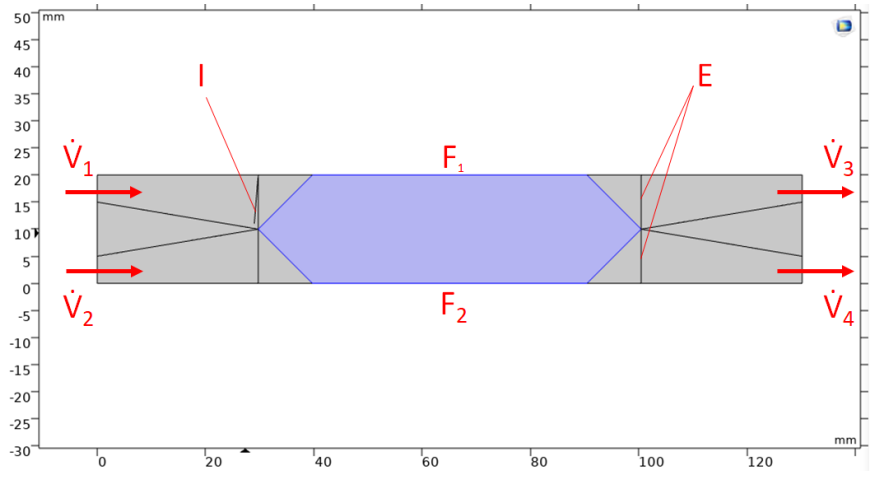

(b) Dual frequency device

Figure 4.12: 2D Geometry COMSOL model. The Acoustic chamber is indicated by the violet coloured region. I - indicates the line of particle release, E - indicates the line of particle exit.

STUDY 1: LAMINAR FLOW

The Navier-Stokes Equation for the given flow were solved to find the velocity field. The boundary conditions were specifed as follows: 1. No slip Condition was specified for the walls. 2. Laminar Outflow with Volumetric flow rates were specified for 3 of the openings $\dot{V}_1$,$\dot{V}_2$,$\dot{V}_3$ & zero pressure

gradient for exit $\dot{V}_4$. The mesh was applied on all the domains; the mesh elements were extremely fine, chosen from the predefined options calibrated for general physics and with minimum element size of 0.00219 mm & maximum of 1.09 mm.

STUDY 2: PARTICLE TRAJECTORIES
The 4 different size distributions mentioned in table 4.1 were created with 200 particles of each distribution with a randomizing function used to generate different sizes within each distribution. The equation of motion of the particles were solved to find their trajectories. The forces specified for the equation of motion were the drag and acoustic radiation force. The inbuilt drag force formulation for inertial regime - Schiller-Naumann - was chosen. The acoustic force was not directly provided. Instead, the pressure field as described in equations 2.10 & 2.4 were provided, along with the acoustic velocity (which was formulated using the impedance relation 2.2). This also means that in case of the dual frequency model, only the vertical component of the field were modelled, and the horizontal component was ignored. The acoustic force was then calculated by COMSOL from these two inputs. The particles were released at a line specified in the particle inlet flow. The final exit for the particles were specified just after the acoustic chamber ended. The mesh used was different for the two forces. The mesh for the drag force was provided in the particle inlet and acoustic chamber domains; the mesh elements were custom defined, with maximum element size equal to wavelength λ or 0.74 µm. The mesh for the acoustic force was provided in the acoustic chamber domain; the mesh elements were custom defined, with minimum element size equal to $\lambda/12$ or 0.06 µm and maximum element size equal to $\lambda/6$ or 0.12 µm. The time step provided was 0.04 s.

RESULTS:
The results of each simulation were the particle sizes and their exact locations, which were then analysed in Matlab to find the particle distribution in each exit. The code for this was also available, provided by H. Kandemir. Minor modifications were done by the author such as incorporating the 4th particle group and writing a small functionality to calculate purity.

ASSUMPTIONS:
There were some assumptions made in the study based on the device and the flow & field conditions. These apply to both simulations and experiments.

1. The geometry and dimensions of the device are such that the flow is laminar throughout, and the flow is fully developed when meeting the acoustic field.
2. Influence of viscosity on the acoustic field can be neglected (Groschl [24]).
3. The shear component of the acoustic field is negligible in comparison to the longitudinal component.
4. The acoustic field is uniform throughout the channel and there are dispersion or attenuation losses.
5. The reflector has perfect reflection.
6. The particle size and main channel dimensions are large enough to neglect acoustic streaming effects (Settnes & Bruus [25]).
7. There are no unsteady effects in the particle motion (Wang et al. [26]).
8. The particle concentration chosen is such that there are no particle-particle interactions (Ley & Bruus [23]).
9. The particles are rigid and neutrally buoyant.

5
RESULTS & DISCUSSION

5.1. OPERATING PARAMETERS

In this section, the chosen values for the different parameters listed in subsection 4.2.7 will be presented. These values were based on both trial simulations as well as experiments.

1. **FLOW RATES**

   Based on the syringe capacities, the possible flow rates were chosen as given in table 5.1. The DOE then forms combinations of the inlet and exit flow rates.

Inlet Flow Rates ($ml\,h^{-1}$)		Exit Flow Rates ($ml\,h^{-1}$)	
Particle Inlet	Water Inlet	Transducer Exit	Reflector Exit
300	700	700	300
400	600	600	400
500	500	500	500

Table 5.1: Selected Flow Rate Values

   From hereon the terms symmetrical flow rates & asymmetrical flow rates will be used for ease of explanation. Symmetrical flow rates refer to the equal flow rate conditions of 500 - 500. Asymmetrical flow rates refer to unequal flow rate conditions of 400 - 600, 600 - 400, 300 - 700, 700 - 300.

2. **OPERATING FREQUENCY**

   The electrical admittance curves of the transducers in both devices, measured in water are give in Fig. 5.1. The range 1.9-2.4 MHz contained higher admittance peaks in all transducers. Hence in frequency sweep device, this was the range used. In case of the dual frequency device, 2.1 MHz was found to be the frequency at which the maximum intersecting admittance value was found, and hence was chosen as the lower operating frequency. The higher operating frequency was then chosen according to the frequency difference given further on in this list. The minor peaks in the frequency sweep device graph are the reflections off the reflector. Such reflections are absent in the dual frequency device because of the presence of sponges.

3. **OPERATING VOLTAGE**

   The voltages in conjunction with the sweep periods and frequency differences, were chosen as $\approx$ 20 V_{pp} (average) for the frequency sweep device & $\approx$ 25 V_{pp} for the dual frequency device. These are values obtained after amplification; the original values set in the waveform generator were: 1.5 V_{pp} & 2 V_{pp} respectively for each device. These values were chosen by setting different flow rate and acoustic field conditions for around 5 trial experiments, and checking the behaviour of the smaller particles; comparatively if too many of the smaller particles do not exit via the reflector, the voltage was deemed better than the others.

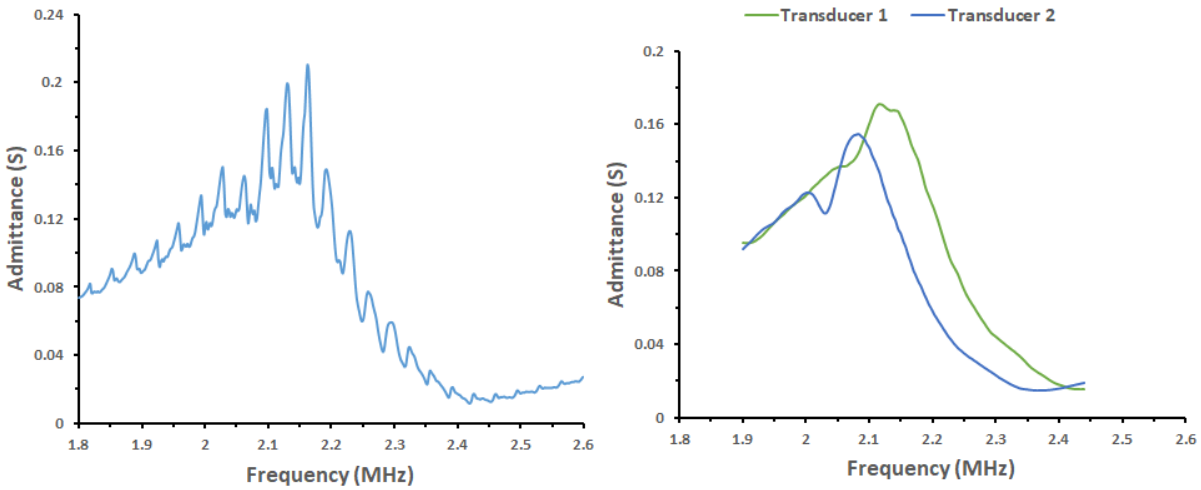

(a) Frequency sweep device

(b) Dual frequency device

Figure 5.1: Electrical Admittance Measurements of the transducers in water

Note: The frequency sweep voltage is presented as an approximate average result, as it was noticed on the oscilloscope that along with the ramping of the frequency, the voltage was also being ramped. The amplitudes also did not vary between the exact same range every time, which is why the average value was found. The dual frequency voltage is also an approximate as it was found that with the application of a frequency difference to one of the excitations, the amplitude of the excitation was found to oscillate. The sources of this behaviour - which could either be in the waveform generator or the amplifier - could not be identified which is why the approximations were used.

4. **PRESSURE MEASUREMENTS**

After find the operating range and the favourable voltage measurements, the LDV pressure amplitude measurements were taken. The entire set of values obtained in Fig. 5.2 - ranging between 40 & 150 kPa - were used for the variable function $P_0(t)$ in the COMSOL model for frequency sweep. For the dual frequency device, the pressure amplitude value at 2.1 MHz was found to be 56.5 kPa. Since only the vertical component of the field is effective in the device, $P_0 \cos 45^\circ$ was calculated as 40 kPa and used in the COMSOL model.

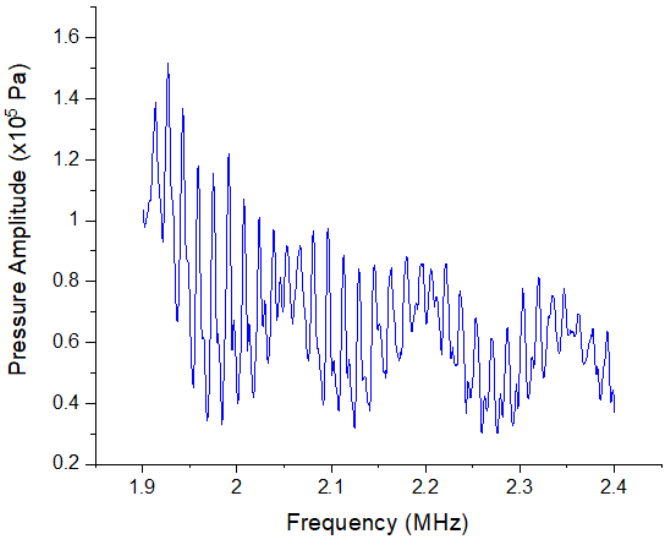

Figure 5.2: Measurements at 25 V_{pp}

5. **SWEEP PERIOD**

   Sweep periods of 1,3,5,7 & 9 s were tested and the favourable ones were found to be 3,5,7 s. With 1 s, the larger particles separated out at short distances, with the particles pushed very close to the reflector surface and moving at very low velocities. The chosen periods 3,5,7 s were such that trajectories have greater inclination towards the direction of drag than the acoustic force, so that particle migration happened over sufficient distance to separate out at the intended exit.

6. **FREQUENCY DIFFERENCE**

   Frequency differences of 1,2,3,4 & 5 Hz were tested, and the favourable ones were found to be 1,2 & 3 Hz. At 4 & 5 Hz difference, the blue particles did follow the nodal movement, but migration over a distance was not observed, instead the particles seem to vibrate in place.

   Supporting images for sweep period and frequency difference can be found in Appendix A.

7. **SUSPENSION CONCENTRATION**

   The concentration chosen was that having equal number of particles of all 4 size distributions. Multiple bottles of this concentration were made over the course of the experiments. The concentration could not be made exact each time, with the error bar being $\pm$ 0.1 g l^{-1}. Below, the concentrations of particles and surfactant that make up the test suspension is given, along with the volume histogram as measured by the particle size analyzer. A representative view of the suspension used in the experiments can be seen in Fig. 5.4.

Colour	Concentration (g l^{-1})
Red	0.03
Cyan	0.08
Orange	0.20
Blue	0.40
CTAB	0.18

Table 5.2: Concentration of Suspension

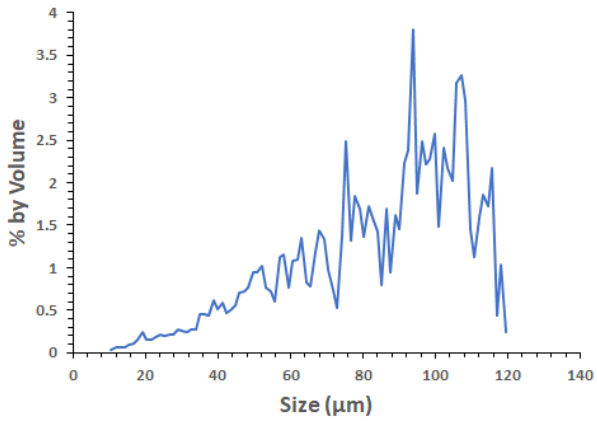

Figure 5.3: Size distribution of Suspension

Figure 5.4: Representative view of the suspension

5.2. FREQUENCY SWEEP

5.2.1. SIMULATION RESULTS

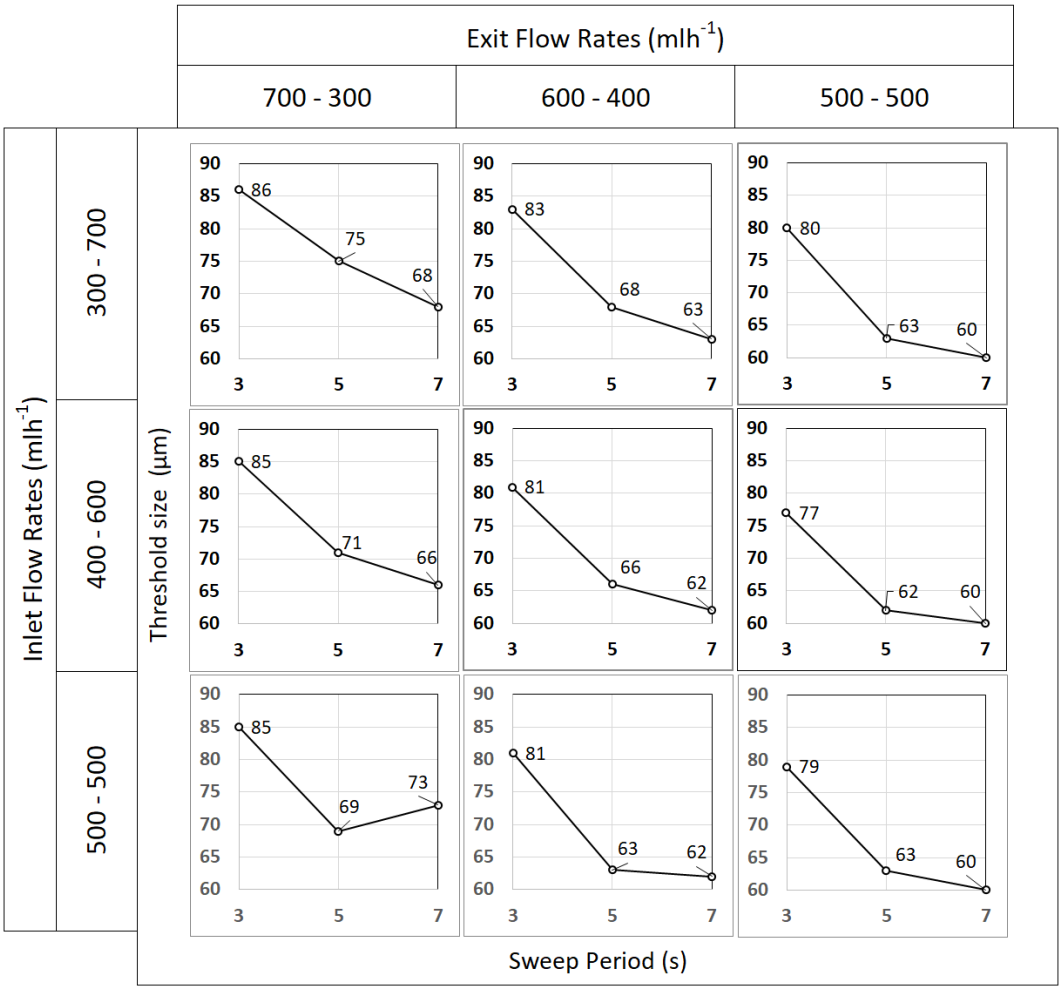

Figure 5.5: Results of the frequency sweep simulations

The results of the simulation are given in figure 5.5. It can be seen that the threshold size of the particles varies from 60-86 µm. The overlap of particle distribution from the transducer exit with the reflector exit (signifying impurity of separation) was less than 10% in all the cases.

EFFECT OF SWEEP PERIOD: It was expected that longer sweep periods would imply that the smaller particles also have the ability to follow the nodes and separate out at the reflector exit, in which case the threshold size would reduce. This can be seen in the results, where the threshold sizes at 7s are mainly between 60-73 µm and the threshold at 3 s are between 75-86 µm. Fig. 5.6 shows the particle trajectories for the same flow rate combinations of 300 - 700 - 500 - 500 ml h^{-1} but at sweep periods of 3 & 7s. The cyan particles in the latter image seem to have crossed over to the reflector exit. The particle trajectories of the orange & blue particles also show that though the smaller particles now follow the nodes due to the increase in sweep period, the trajectory of the bigger particles show that they do not follow the nodal movement as easily in comparison to 3 s & 5 s, which was not anticipated. This response can be visualised by finding when the bigger particles reach the reflector wall; in the former case it reaches the reflector wall in the acoustic chamber, while in the latter it does not reach the reflector wall at all.

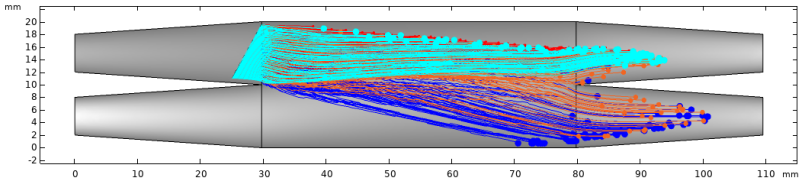

(a) Particle Trajectories at 3s Sweep Period

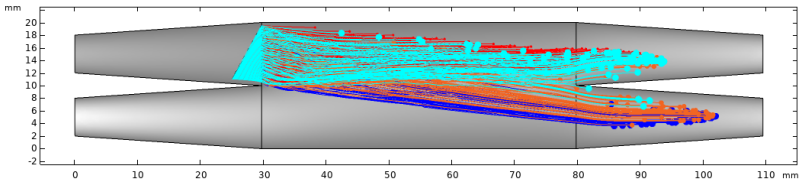

(b) Particle Trajectories at 7s Sweep Period

Figure 5.6: Particle Trajectories from the results of simulations to visualise the effect of sweep periods. The inlet flow rates are 300 - 700 ml h^{-1} and exit flow rates are 500 - 500 ml h^{-1}.

EFFECT OF EXIT FLOW RATE: The exit flow rates seem to have a great influence on the threshold size. A particle that is migrating towards the reflector end, will pass through either of the exits depending on its exact position and the way the streamlines are curved at the end of the acoustic chamber. Exit flow rates of say 700-300 ml h^{-1} would have streamlines curved towards the transducer outlet, as opposed to exit flow rates of 500-500 ml h^{-1} where the the streamlines are symmetrical at the exit because of the equal flow rate, refer Fig. 5.7. This would mean that a large particle near the exit guideway, say at location (75,8) mm would be more likely to leave via the transducer exit in case of 5.7b and more likely to leave via the reflector exit in case of 5.7a. This can be seen in the Particle Trajectories in Fig. 5.8. Notice the predominant upward movement of the larger particles in Fig. 5.8b as compared to their downward movement in Fig. 5.8a. This in turn implies that an increase in the transducer flow rate would increase the threshold size, as can also be seen in the results.

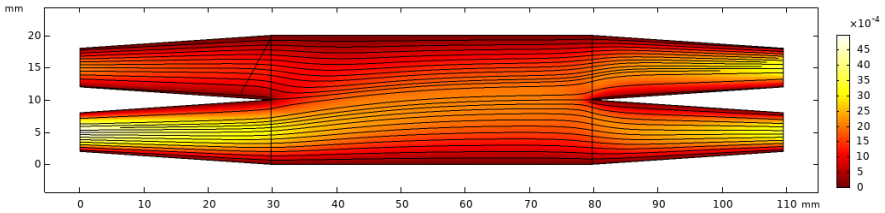

(a) Streamlines for the exit flow rates of 500 - 500 ml h^{-1}

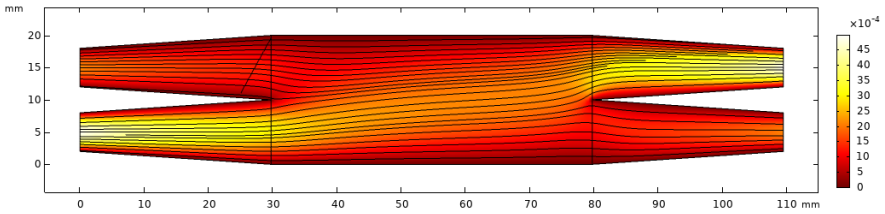

(b) Streamlines for the exit flow rates of 700 - 300 ml h^{-1}

Figure 5.7: Streamlines from the results of simulations to visualise the effect of exit flow rate. The inlet flow rates are 300 - 700 ml h^{-1}.

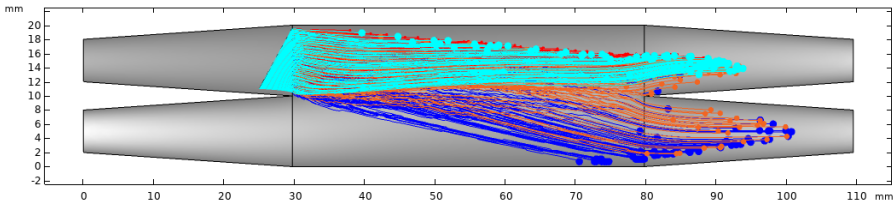

(a) Particle Trajectories for the exit flow rates of 500 - 500 ml h^{-1}

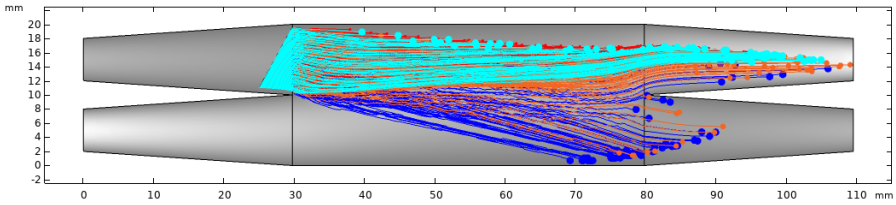

(b) Particle Trajectories for the exit flow rates of 700 - 300 ml h^{-1}

Figure 5.8: Particle Trajectories from the results of simulations to visualise the effect of exit flow rate. The inlet flow rates are 300 - 700 ml h^{-1} and sweep period is 3 s.

EFFECT OF INLET FLOW RATE: The curvature of the streamlines are influenced not only by the exit flow rates, but also by the inlet flow rates. Also, the acoustic force affects the smaller particles, causing them to deflect towards the reflector, even if they don't follow the nodal pattern. This might cause them to exit via the reflector. The higher water inlet ensures that the particle stream is kept closer to the transducer surface, forcing the smaller particles to exit via the transducer outlet rather than the reflector. The streamlines in Fig. 5.9b help visualise the narrowing of the particle stream in response to the greater water inlet stream, for equal exit flow rates. Cyan particles can be seen exiting the reflector outlet in the symmetrical inlet flow rate, while entirety exits via the transducer outlet in case of the higher water inlet flow rate.

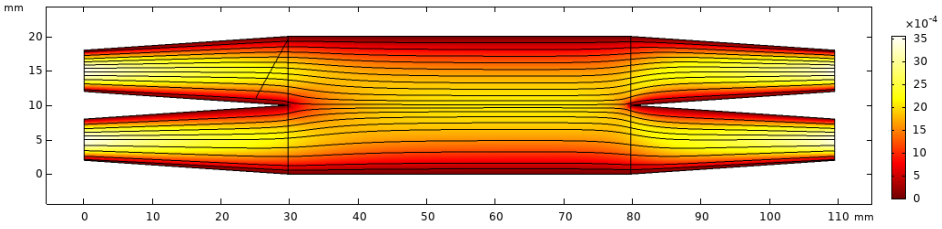

(a) Streamlines for the inlet flow rates of 500 - 500 ml h^{-1}

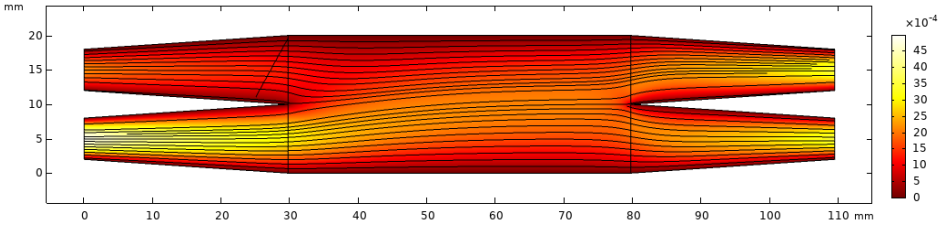

(b) Streamlines for the inlet flow rates of 300 - 700 ml h^{-1}

Figure 5.9: Streamlines from the results of simulations to visualise the effect of inlet flow rate. The exit flow rates are 500 - 500 ml h^{-1}.

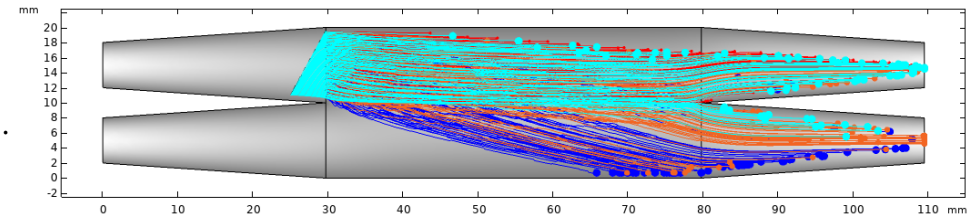

(a) Particle Trajectories for the inlet flow rates of 500 - 500 ml h^{-1}

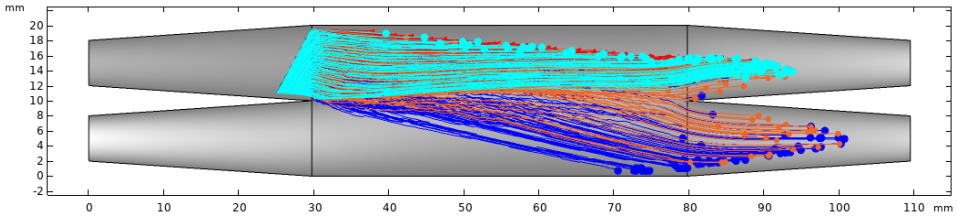

(b) Particle Trajectories for the inlet flow rates of 300 - 700 ml h^{-1}

Figure 5.10: Particle Trajectories from the results of simulations to visualise the effect of inlet flow rate. The exit flow rates are 500 - 500 ml h^{-1} and sweep period is 3 s

Although the individual trends can be reasoned out, the competitiveness of each parameter with respect to the other, and how they together contribute to the separation process can only be understood by means of a DOE analysis.

5.2.2. DOE ANALYSIS FOR SIMULATIONS

Presented below are the main results from which parallels can be drawn with the reasoning in the previous subsection.

PARETO CHART:

Only the sweep period and the exit flow rates are significant. Even then, the sweep period seems to have a significantly higher effect than the exit flow rates as can also be seen in the effects chart. There are no significant interaction effects in the model.

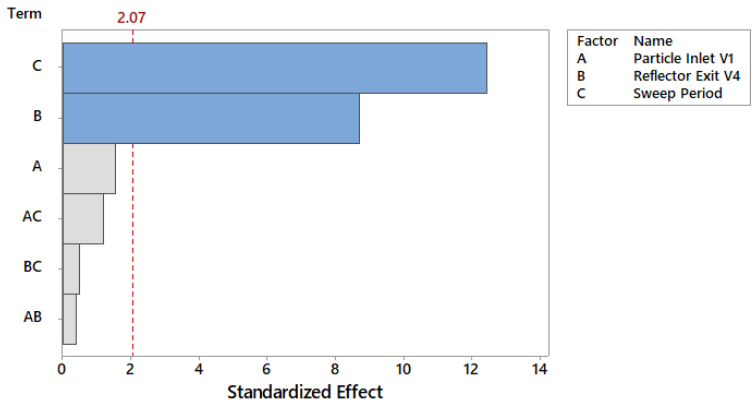

Figure 5.11: Pareto Chart of Standardized Effects. The blue bars represent significant factors, while the grey bars are insignificant.

MAIN EFFECTS:

As the exit flow rates become symmetrical, the threshold size decreases. The decrease can also be seen in the increase in sweep period. In addition, there is a significantly greater decrease between 3 & 5 s than between 5 & 7 s, implying perhaps a greater response of the system towards the former two sweep periods, than towards 7 s, a point which was also noted in 5.6b.

Figure 5.12: Main Effects Chart for simulation results

5.2.3. EXPERIMENT RESULTS

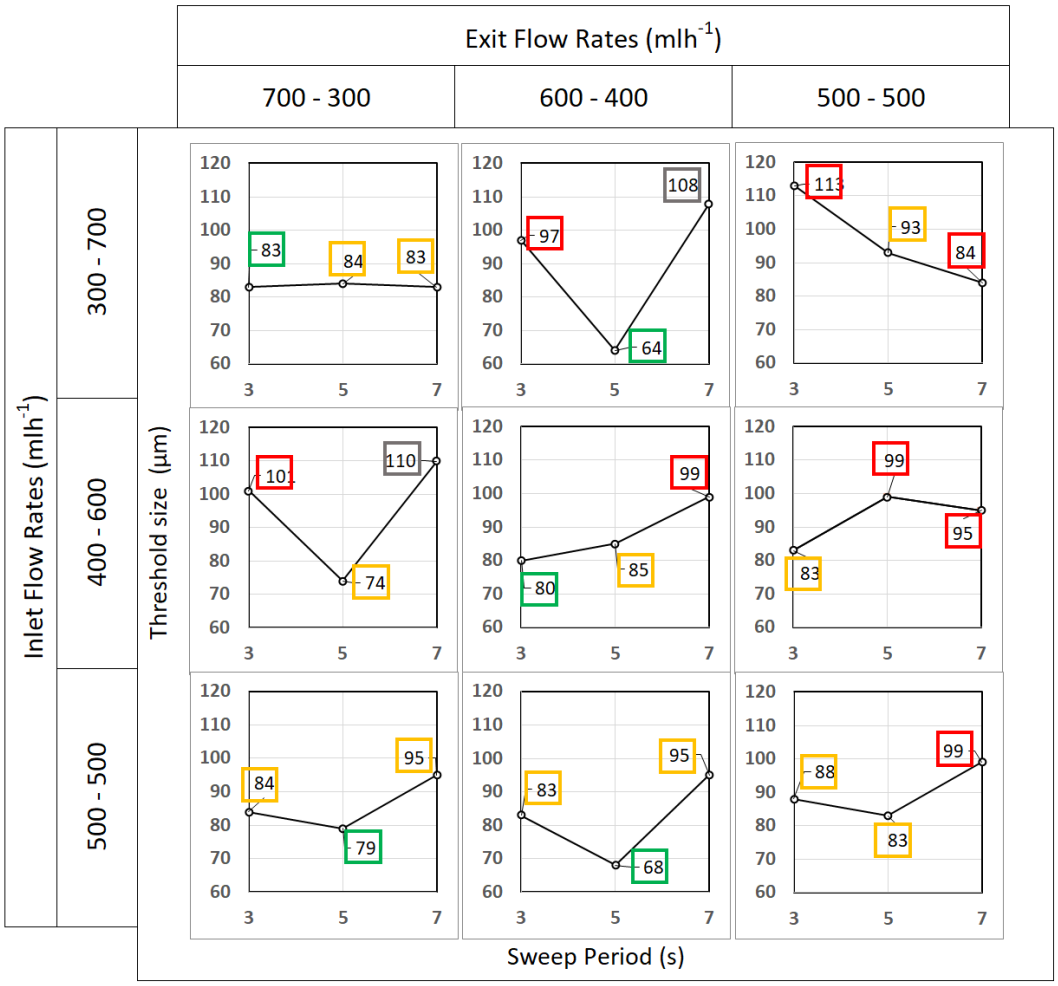

Figure 5.13: Results of frequency sweep experiments
Purity Scale: Green boxes - >50%, Yellow boxes - 30-50%,
Red boxes - <30%, Grey boxes - no separation

The threshold for separation varies between 64-100 µm with most of the separation happening between the 80-100 µm range. The overlap of particle distribution in the transducer exit with the

reflector exit is significant in all the cases (i.e. impurity is >30%), unlike in the simulations. The maximum purity of ~68% obtained when the conditions are 300 - 700 - 600 - 400 ml h^{-1} and sweep period is 5s.
It can be seen that the sweep period of 5 s is the best performing, closely followed by that of 3 s. 7 s does not perform well in comparison. With respect to flow rate parameters, the inlet flow rates of 500 - 500 ml h^{-1} & exit flow rates of 700 - 300 ml h^{-1} seem to perform well, when comparing the number of experiments that resulted in separation purity >30%; there is no distinct trend to be drawn however, as those are also scattered among different conditions. A clearer picture can be obtained by the DOE analysis.

5.2.4. DOE ANALYSIS FOR EXPERIMENTS

PARETO CHART: In the chart 5.14, the sweep period seems to be the only effective parameter.

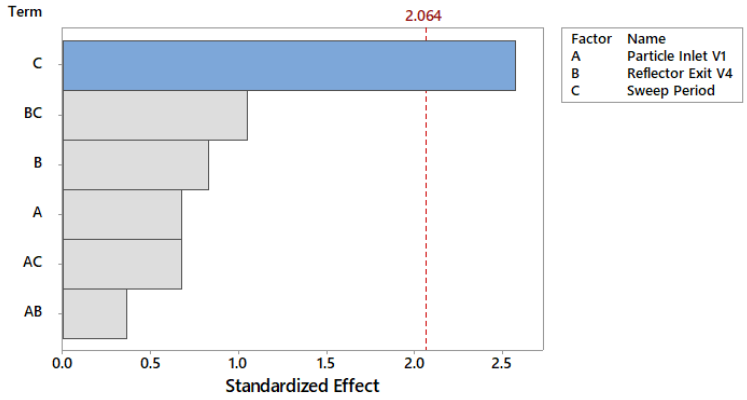

Figure 5.14: Pareto Chart of Standardized Effects.
The blue bars represent factors that have significant effects, while the grey bars are factors that are insignificant.

MAIN EFFECTS: The decrease in size between 3 & 5 s sweep periods is as expected. The increase in threshold size for the 7 s sweep period can be explained by the decreased response of the larger particles to this sweep period (as was also seen in the simulations). The decreased response results in some of the larger particles following the nodal movement while some don't, allowing particles to leave via both exits and hence increasing threshold size.

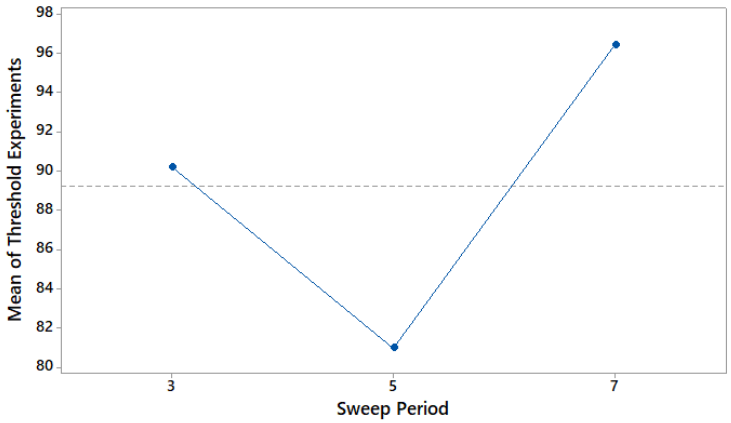

Figure 5.15: Main Effects Chart for simulation results

5.2.5. PARTICLE SIZE DISTRIBUTIONS

Given below is a comparison of the PSD graphs from the simulations and experiments, for all the conditions where the purity of separation in the experiments is >50%. There are a few points that need to be mentioned:

- The initial PSD given for the experiments, was the measurement taken at the start of the DOE. However, the PSD was not measured at the start of every run. As mentioned before, the suspension was constantly stirred to ensure uniform distribution of the particles during each run. The initial PSD in the graphs is therefore a good estimate, but not the exact distribution at each run.

- Particles of larger sizes of ~ 100 µm are absent in some of the PSDs. This could be due to the tendency of the larger particles to stick to the channel walls. In addition, DIPA requires sufficient number of particles to plot the histogram with sufficient confidence. Added to this, the averaging of the PSDs across the 3 measurements could imply elimination of the larger sized particles from the final plot if they are not sufficient in volume.

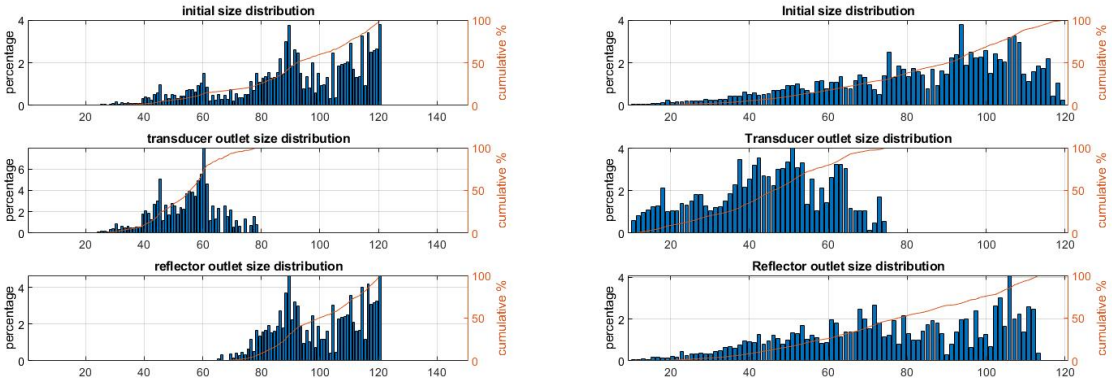

(a) Simulations
Purity:99.56%

(b) Experiments
Purity: 68%

Figure 5.16: Particle Size Distribution for the conditions 300 - 700 - 600 - 400 ml h^{-1} & 5 s sweep period

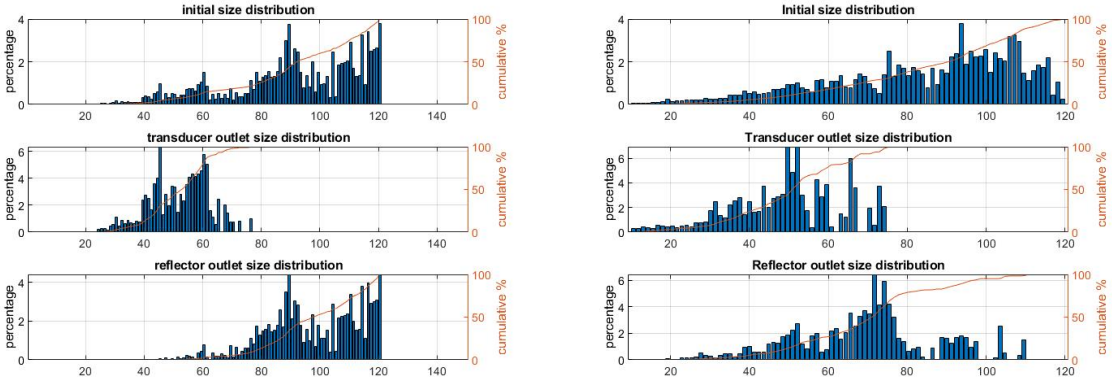

(a) Simulations
Purity: 97%

(b) Experiments
Purity: 58%

Figure 5.17: Particle Size Distribution for the conditions 500 - 500 - 600 - 400 ml h^{-1} & 5 s sweep period

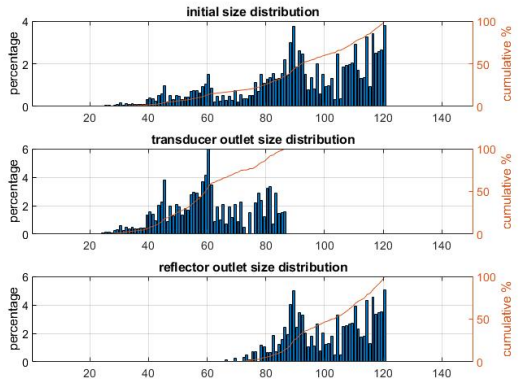

(a) Simulations
Purity: 94.3%

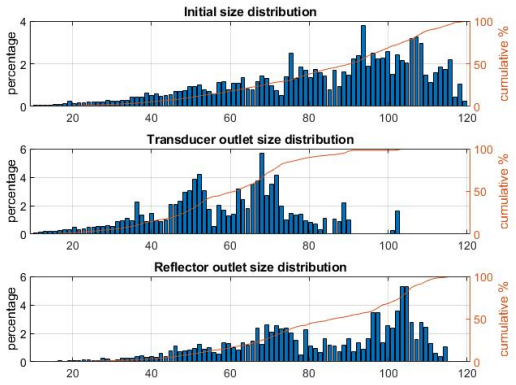

(b) Experiments
Purity: 55%

Figure 5.18: Particle Size Distribution for the conditions 400 - 600 - 600 - 400 ml h^{-1} & 3 s sweep period

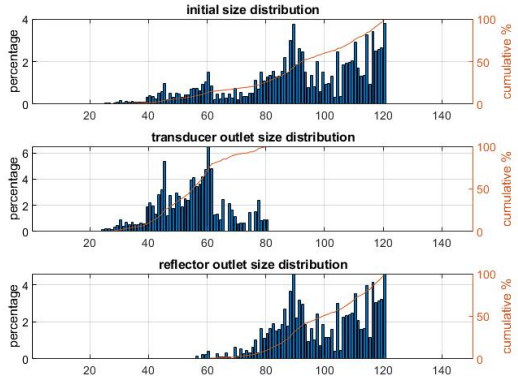

(a) Simulations
Purity: 98%

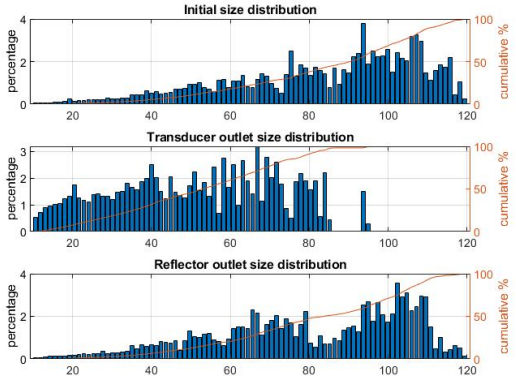

(b) Experiments
Purity: 54%

Figure 5.19: Particle Size Distribution for the conditions 500 - 500 - 700 - 300 ml h^{-1} & 5 s sweep period

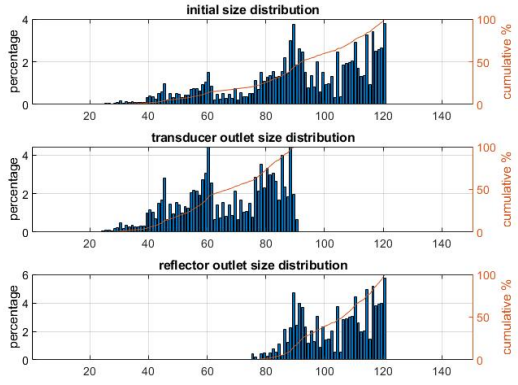

(a) Simulations
Purity: 95%

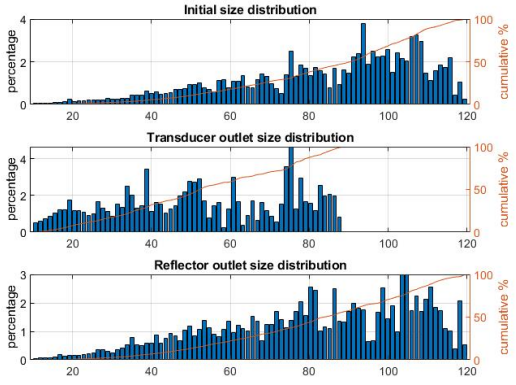

(b) Experiments
Purity: 51%

Figure 5.20: Particle Size Distribution for the conditions 300 - 700 - 700 - 300 ml h^{-1} & 3 s sweep period

5.3. DUAL FREQUENCY

5.3.1. SIMULATION RESULTS

While performing the simulations for this device, it was noted that a lot of the larger particles did not migrate to the reflector end unlike in the frequency sweep device, and the PSD was very different in comparison. The PSD overlap of the transducer with the reflector was very high, yielding a reflector impurity of 70%, as opposed to a 10% impurity in the frequency sweep device. Hence it was decided that for this device, the D10 size would be used for finding out the threhold size. The impurity of the transducer samples was then found to vary between 9-46%.

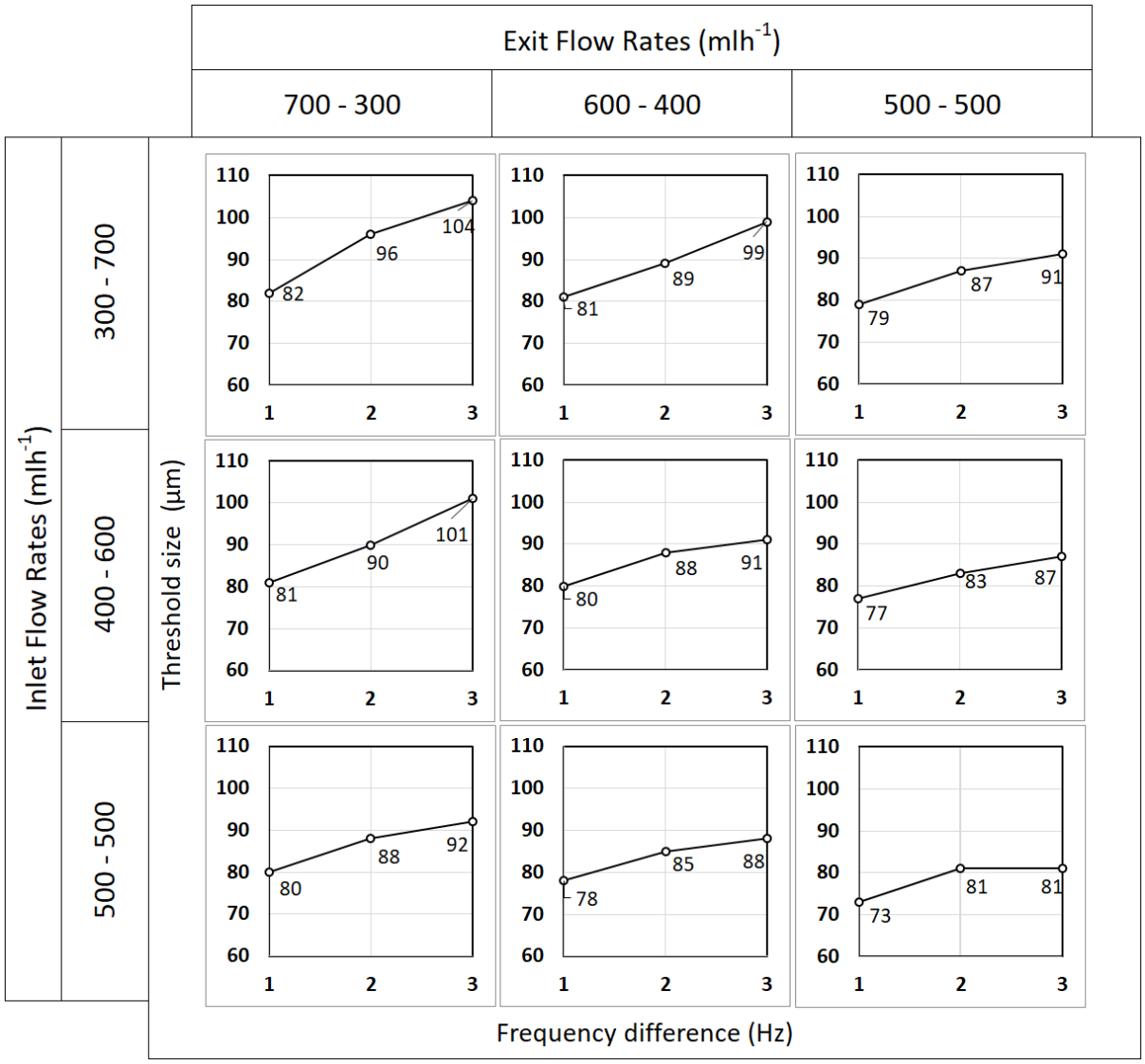

Figure 5.21: Results of dual frequency simulations

The threshold size for separation varies between 73-104 µm.

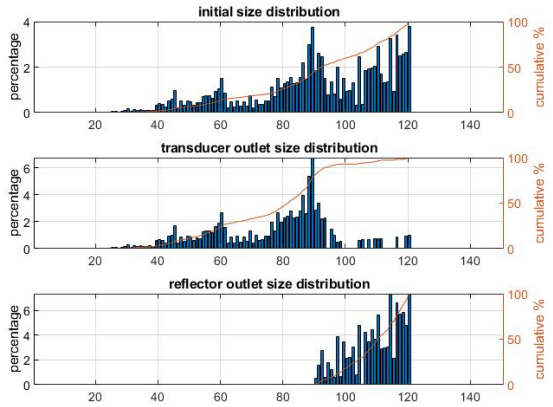

(a) 300 - 700 - 700 - 300 ml h^{-1} - 2 Hz Frequency Difference. Purity: 91%

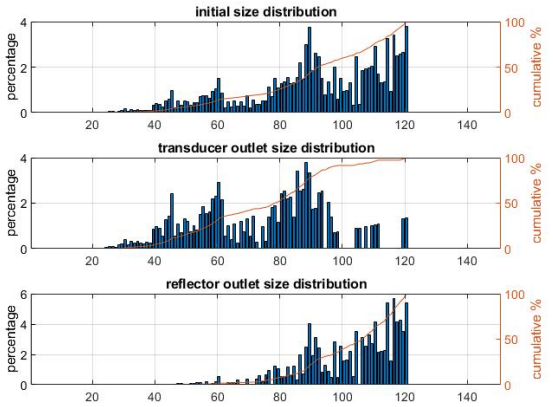

(b) 500 - 500 - 500 - 500 ml h^{-1} - 3 Hz Frequency Difference. Purity: 54%

Figure 5.22: Particle Size Distribution graphs for dual frequency device showing the conditions with least and maximum impurity

EFFECT OF FREQUENCY DIFFERENCE: A similar line of reasoning followed for the frequency sweep device can also be used here. It was expected that a smaller frequency difference would imply that the smaller particles also have the ability to follow the nodes and separate out at the reflector exit, in which case the threshold size would be small. As the frequency difference is increased, only the larger ones can follow and hence only they can separate out at the reflector exit. This can indeed be seen in the results in the results; for every flow rate combination, the threshold sizes increases as the frequency difference increases.

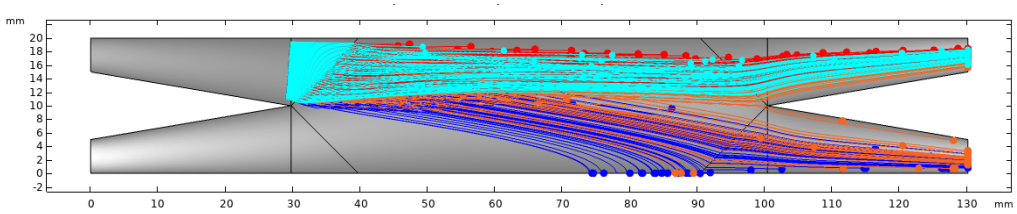

(a) Particle Trajectories at 1 Hz Frequency Difference

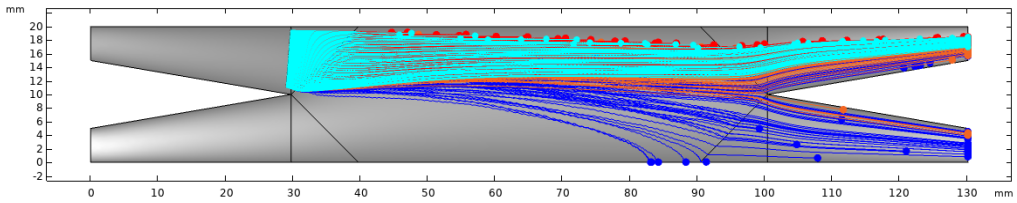

(b) Particle Trajectories at 3 Hz Frequency Difference

Figure 5.23: Particle Trajectories from the results of simulations to visualise the effect of Frequency Difference. The inlet flow rates are 300 - 700 ml h^{-1} and exit flow rates are 500 - 500 ml h^{-1}.

EFFECT OF EXIT FLOW RATES: Similar to the frequency sweep device, it is expected that the exit flow rates would contribute to the threshold size. With the same reasoning, the upward curving of the streamlines at the exit influences the particle movement. The streamlines can be viewed in Fig. 5.24, and the particle trajectories in Fig. 5.25. This in turn implies that an increase in the transducer flow rate would increase the threshold size, as can also be seen in the results.

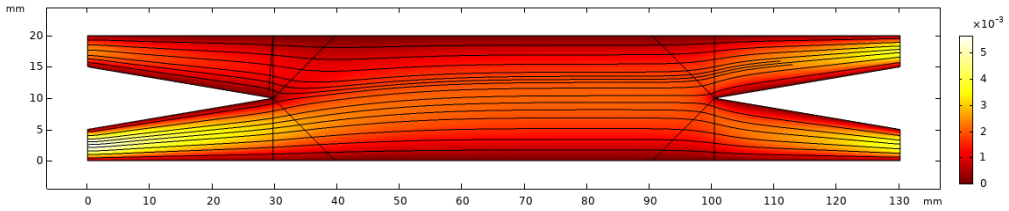

(a) Streamlines for the exit flow rates of 500 - 500 ml h^{-1}

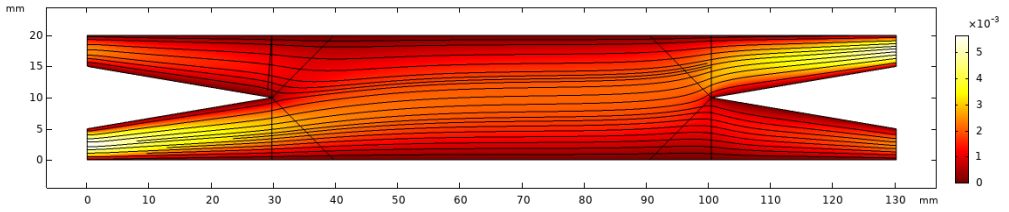

(b) Streamlines for the exit flow rates of 700 - 300 ml h^{-1}

Figure 5.24: Streamlines from the results of simulations to visualise the effect of exit flow rate. The inlet flow rates are 300 - 700 ml h^{-1}.

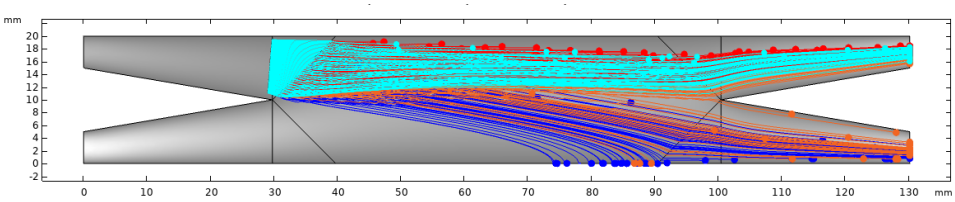

(a) Particle Trajectories at exit flow rates of 500 - 500 ml h^{-1}

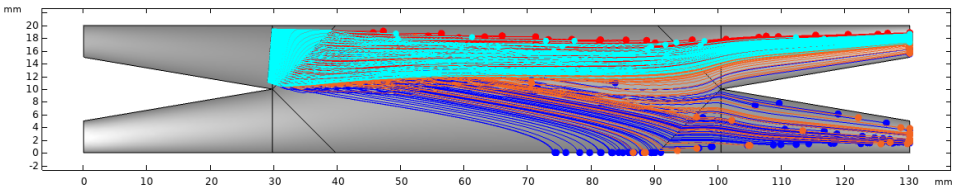

(b) Particle Trajectories at exit flow rates of 700 - 300 ml h^{-1}

Figure 5.25: Particle Trajectories from the results of simulations to visualise the effect of exit flow rate. The inlet flow rates are 300 - 700 ml h^{-1} and frequency difference is 1 Hz.

EFFECT OF INLET FLOW RATES: The inlet flow rates in this device are also expected to influence particle behaviour in the same way. The higher water inlet ensures that the particle stream is kept closer to the higher frequency surface forcing the exit of the smaller particles via the transducer exit rather than the reflector. Fig. 5.27 illustrates this effect.

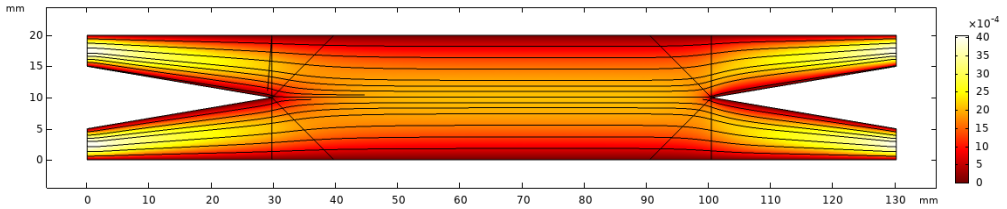

(a) Streamlines for the inlet flow rates of 500 - 500 ml h^{-1}

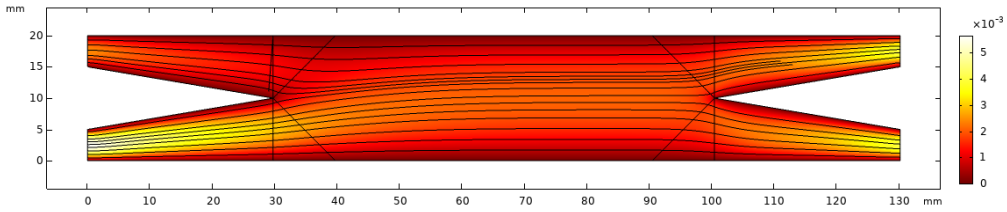

(b) Streamlines for the inlet flow rates of 300 - 700 ml h^{-1}

Figure 5.26: Streamlines from the results of simulations to visualise the effect of inlet flow rate. The exit flow rates are 500 - 500 ml h^{-1}.

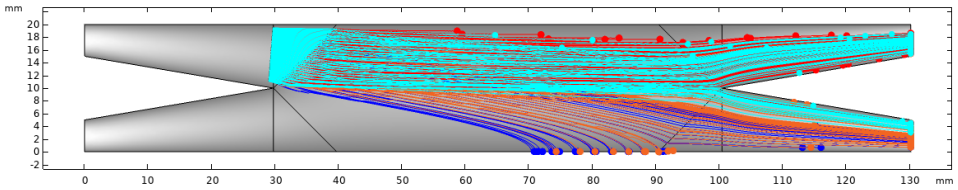

(a) Particle Trajectories for the inlet flow rates of 500 - 500 ml h^{-1}

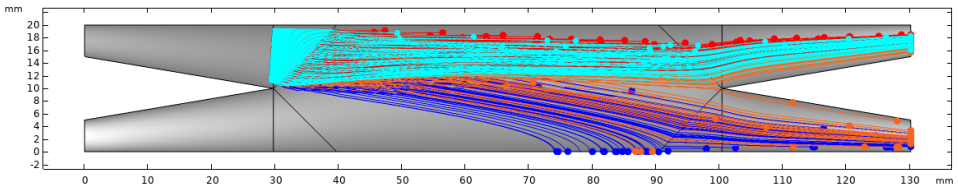

(b) Particle Trajectories for the inlet flow rates of 300 - 700 ml h^{-1}

Figure 5.27: Particle Trajectories from the results of simulations to visualise the effect of inlet flow rate. The exit flow rates are 500 - 500 ml h^{-1} and frequency difference is 1 Hz

5.3.2. DOE ANALYSIS FOR SIMULATIONS

PARETO CHART: The Pareto chart for dual frequency Fig. 5.28 shows a similarity to that of frequency sweep, in terms of the greatest effects being the frequency difference followed by the exit flow rates. In addition, the inlet flow rates are also significant; also significant are the interaction effects of the frequency difference with both exit and inlet flow rates.

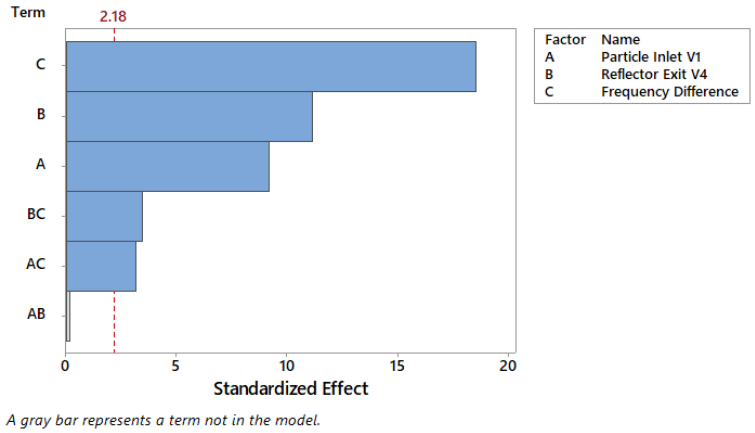

Figure 5.28: Pareto Chart for simulation results

MAIN EFFECTS: The effects trends are as expected, with the inlet and exit flow rates having a decreasing trend of threshold size with increase of flow symmetry, and the frequency difference having an increasing trend of threshold size with increase in the difference.

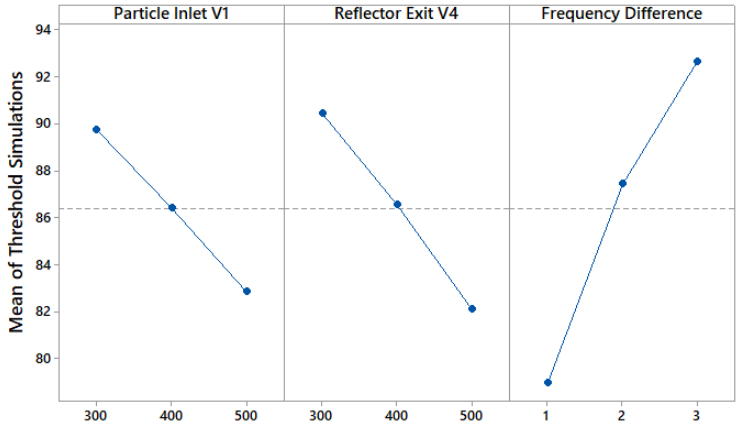

Figure 5.29: Main Effects Chart for simulation results

INTERACTION EFFECTS: The effect of frequency difference on different inlet and exit flow rates, can be seen in plots 5.30a & 5.30b respectively. For every flow rate condition, the increase in frequency difference leads to an increase in threshold size (as can be seen in each of the individual curves). Furthermore, in each plot it can be see that as the flow rates become asymmetrical, the curves move upward in the plot i.e. the threshold size increases.

Complementary to this, the effect of different inlet and exit flow rates on the frequency difference can be seen in plots 5.31a & 5.31b respectively. For all frequency difference conditions, the threshold size decreases as the flow rates become symmetrical. Furthermore, with an increase in the frequency difference, the curves move upward in the plots i.e. the threshold size increases.

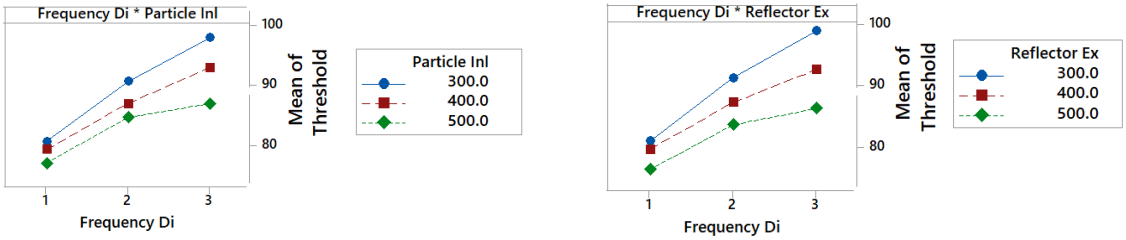

(a) Effect of frequency difference on the inlet flow rates

(b) Effect of frequency difference on the exit flow rates

Figure 5.30: Interaction effects: Effect of Frequency difference

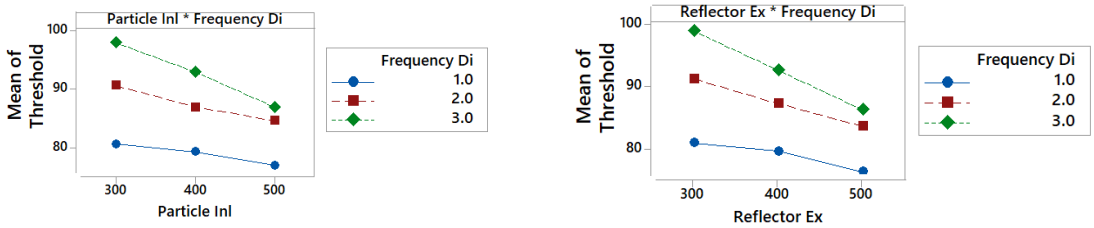

(a) Effect of inlet flow rate on the frequency difference

(b) Effect of exit flow rate on the frequency difference

Figure 5.31: Interaction effects: Effect of Flow rates

5.3.3. EXPERIMENTS

To check if the dual frequency device does not have reflections and serves its intended purpose, a standing wavefield was created at 2.1 MHz in the dual frequency device. The frequency sweep device was repurposed to fit in two transducers and the standing wavefield was again created at 2.1 MHz. On comparing both figures in 5.32, the former showed clear patterns of particles trapped at the nodes and followed a straight trajectory. The latter showed zigzag patterns from the reflection effects. It was then concluded that reflection effects can indeed be ignored in this device.

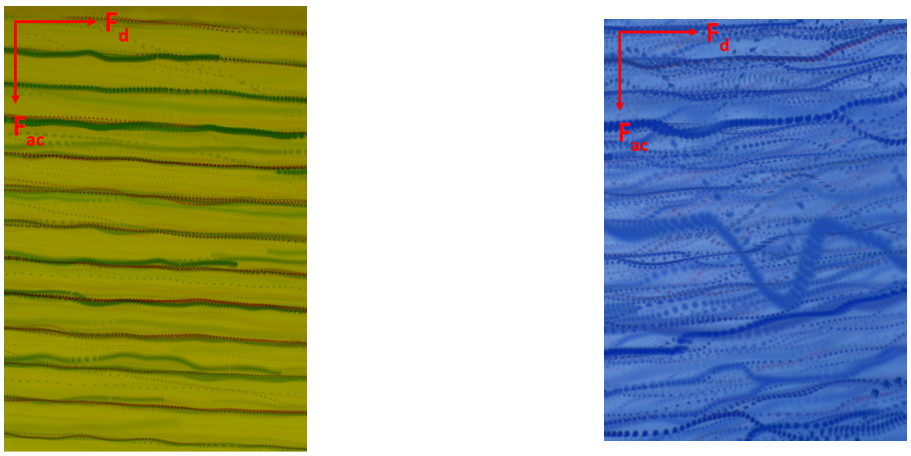

(a) Perpendicular orientation

(b) Face-to-face orientation

Figure 5.32: Comparison of standing wave field at 2.1 MHz in a dual frequency configuration, for different transducer orientations.

Around 8 DOE experiments for this device was carried out, during which it was found that the device had a few problems that lead to no separation. This was also confirmed with the particle size analysis of the samples, 5 of which are represented here. Although poor separation was also observed in some of the frequency sweep experiments, the problems that manifested in this device were such that it was

concluded that this device would not be capable of separating particles. The problems identified can be found in Appendix B.

As can be seen in the figures, there is no distinction of the PSD curves in either the transducer or reflector samples.

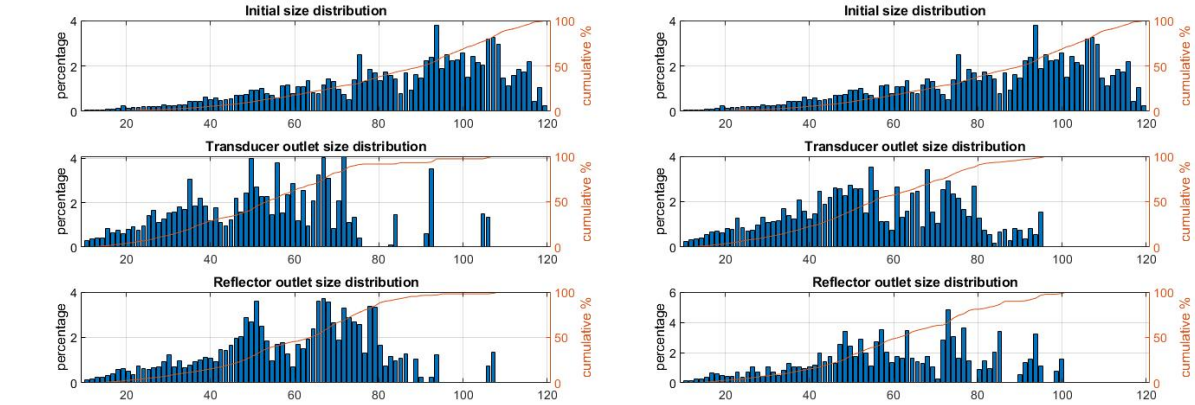

(a) 300 - 700 - 500 - 500 ml h^{-1} - 2Hz Frequency Difference. (b) 300 - 700 - 500 - 500 ml h^{-1} - 3Hz Frequency Difference.

Figure 5.33: Particle Size Distribution graphs for dual frequency device Experiments

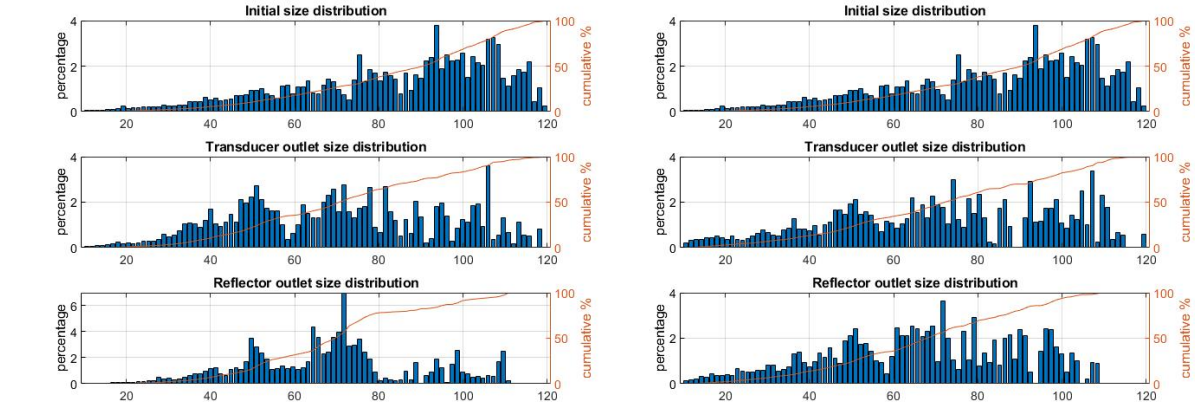

(a) 500 - 500 - 600 - 400 ml h^{-1} - 1Hz Frequency Difference. (b) 500 - 500 - 600 - 400 ml h^{-1} - 2Hz Frequency Difference.

Figure 5.34: Particle Size Distribution graphs for dual frequency device Experiments

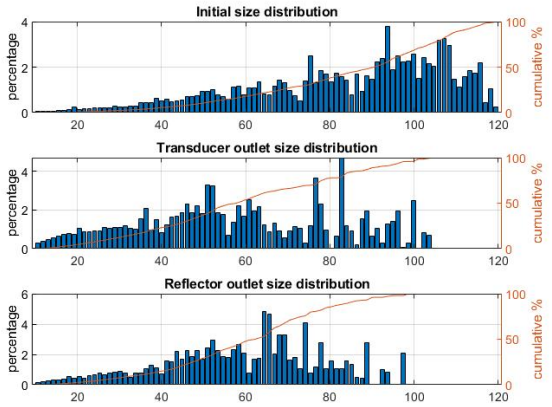

Figure 5.35: Particle Size Distribution graphs for dual frequency device Experiments.
The conditions are 400 - 600 - 600 - 400 ml h^{-1} & 2 Hz

5.4. GENERAL DISCUSSIONS:

As was seen in the previous sections, the results of the simulations deviated from those of the experiments, though the threshold sizes were in the same range. A few of the possible reasons have been given below:

1. The pressure distribution provided to the model was also not exact, as the actual variation of pressure caused by the transducers is difficult to be captured. There could be different factors causing this, such as fluctuations in power input and the functioning of the transducers themselves varying with time. Also, as mentioned earlier, the same transducers could not used constantly due to wire disconnections, resulting in their being replaced often. This results in the pressure amplitude captured by the LDV being just an estimate of its behaviour, and not a real time value.

2. Problems were also encountered in the flow; frequent of them were pulsations due to either the ill-fitment of syringes in the pumps causing a relative motion between the syringe and pump, or the presence of air bubbles in the tubes. Of note was also a minor circulation along the exit guideway, from the transducer exit to the reflector exit which happenend even with symmetric exit flow rates. On occasion, a slight fluctuation in the flow rate was detected at the start of the experiment which usually corrected itself. When the above problems occurred, the experiments were stopped and repeated; but there were also cases were this could not be prevented, and the samples captured were used as is.

6

SUMMARY & RECOMMENDATIONS

Selective particle separation using Dynamic Acoustic Fields on a large scale (1000 mL h^{-1}) has been exhibited on a particle size range of 32-106 μm using the frequency sweep device. The threshold size varied between 60-86 μm in the simulations, and between 80-100 μm in the experiments. The sweep periods were the parameters that showed maximum effects on the threshold sizes in both simulations and experiments. Exit flow rates had significant effects on the threshold size in the simulations; disturbances in the flow could be a reason why the flow rates are not the main influencers in the experiments. In the dual frequency device, the simulations showed threshold size variation between 73-104 μm, with all parameters effecting the threshold size. The dual frequency device did not exhibit separation in the experiments due to problems in the acoustic field, the causes for which could not be identified.

The novelty of the separation shown in the frequency sweep device comes from the fact that separation of this wide a range of particles on a large scale has not been demonstrated using DAF before. Literature has shown separation of set of fixed particle sizes (for e.g. separation of a mixture of particles sized 2 & 10 μm) and not a range as demonstrated here. The sizes demonstrated in literature are seldom higher than 50 μm. The difficulty in separation of a wide range as opposed to separation of fixed sets of sizes is that, while exact tuning conditions for separation can be set in the latter, in the former this cannot be done. Setting of exact operating condition in case of fixed sizes would mean a binary yes or no reaction, which would mean identifying whether the particles react favourably to the conditions or not, so that they exit via their intended outlets. In case of a range, the operating conditions would result in a scale of reactions, with each size having its own affinity towards the conditions. An added difficulty of trying to separate larger sizes is their tendency to stick to the walls, as opposed to smaller sized particles.

There is great scope in future research in the DAF devices. With the current conditions, it was seen that separation happened only at the larger sizes (≈ 70-80 μm), than at the smaller sizes (≈ 40-50 μm), which could very well be the greater drag forces acting on the smaller range. This would mean a further reduction in the drag force or lower channel flow rates could help separation in the smaller sizes. Variations in geometry such as, moving the inlet separation guideway closer to the reflector wall, could aid formation of a thinner particle layer. Similar variations in exit guideway positions can also be tested. Also, slight modifications in the setup can be made, such as the provision for a longer duration of experiment run. Currently each experiment takes ≈ 5 mins at which the syringes run out. If reservoirs rather than syringes can be incorporated in the flow network, larger flow rates and longer experiment runs can be tested (although care should be taken to stay in the low inertial regime). Flow meters can be incorporated in the flow network to constantly monitor the pump. Lower concentrations of the suspension also need to be tested to see if separation purity improves. This also implies finding a different means of measuring particle sizes. For the excitations, rest and ramp cycle, as seen in literature could be applied. In the dual frequency device, the causes as to the behaviour of the acoustic field need to be studied. Different angular positions of the transducers can also be tried out to create new devices, to see if separation occurs without reflections in the field.

A

Additional Results

SELECTION OF SWEEP PERIOD:

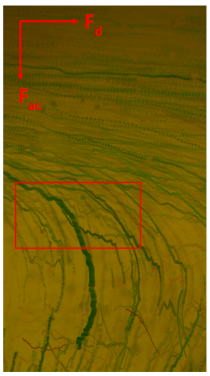

(a) 1s

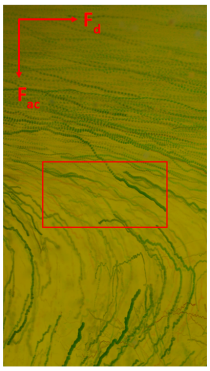

(b) 3s

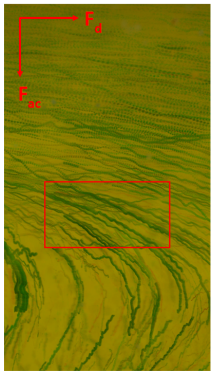

(c) 5s

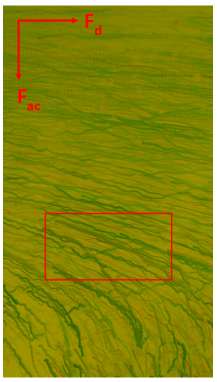

(d) 7s

Figure A.1: Stack images of some sweep period trials.
Selecting sweep periods can be done by observing the slope of the blue particle trajectories nearest to the main particle inlet flow.

SELECTION OF FREQUENCY DIFFERENCE:

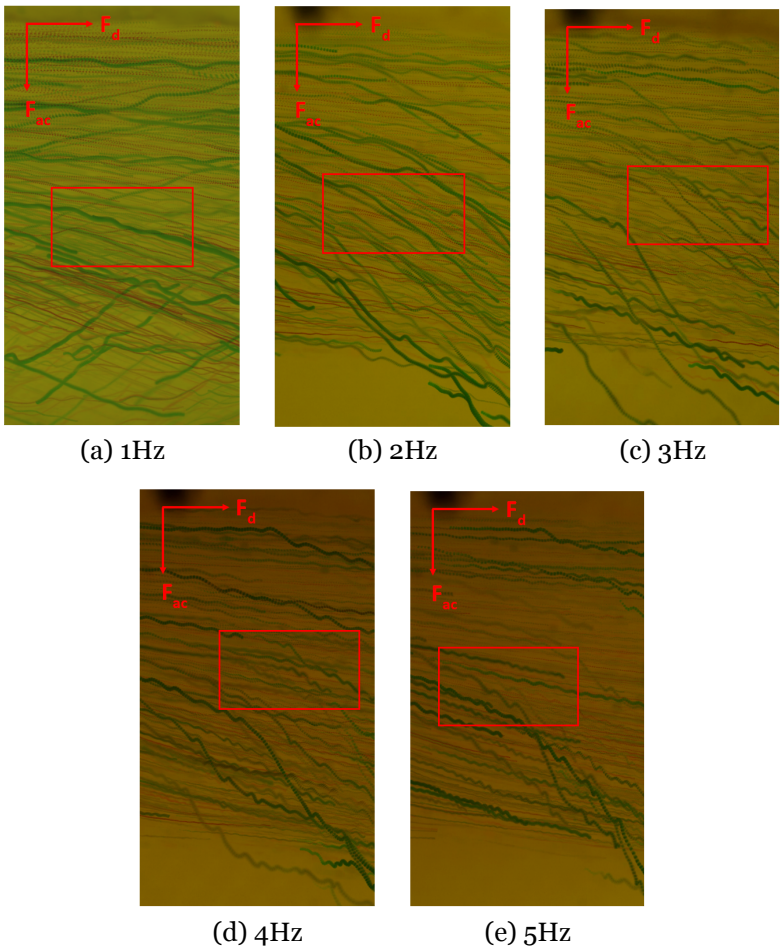

(a) 1Hz (b) 2Hz (c) 3Hz

(d) 4Hz (e) 5Hz

Figure A.2: Stack images of some frequency difference trials.
Observing the slope of the trajectories of the blue particles, shows the first three values to be suitable. The latter two seem to have higher zigzags indicating particles might be vibrating in place but not migrating

B

DUAL FREQUENCY DEVICE

The problems faced have been listed out as follows:

1. It was found that while separation happened during the start of the experiment, after approximately a minute, the field seemed to stop 'working', and the particles instead of migrating across the channel, simply follow the streamlines. The images for this phenomenon has been shown in B.1. When this happened, the transducers were also checked by immediately switching to a standing wave field at 2.1 MHz, which was created perfectly as before, which lead to the conclusion that it was not the fault of the transducers.

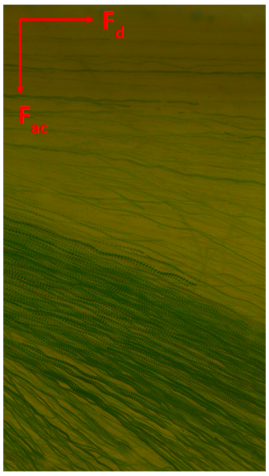

(a) Separation at the start of the experiment

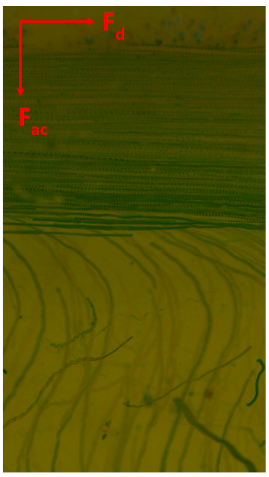

(b) Separation after approx. 1 minute. Particles merely follow streamlines.

Figure B.1: Irregular working of the field.

2. Of the particles that migrated across the channel, there seemed to be a 'reverse migration' at the end of the acoustic chamber, where the particles move back to the particle inlet flow. In Fig. B.2, the straight arrow gives the trajectories of the particles that are separating as intended, and the curve arrow gives the trajectories where the particles can be seen trying to migrate back to the original particle flow stream.

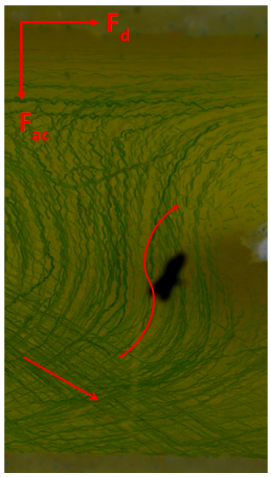

Figure B.2: Reverse migration of particles at the end of the acoustic chamber.

3. At the mid plane of the channel and along the length of the acoustic chamber, the larger particles (orange & blue) were found to be trapped and oscillating about a fixed point. In Fig. B.3, the red boxes highlights the regions where blocks can be seen instead of lines, indicating the particles oscillating in the fixed regions instead of migrating.

4. The oscillation of the particles, in a lot of cases, lead to aggregation as more of the particles got trapped in these locations as time progressed. These aggregates mostly remain at these locations, but more often they detach and pass through one of the exits. Here the aggregates can be seen in Fig. B.4 exiting through the reflector outlet.

Figure B.3: Oscillation of the particles at the mid plane.

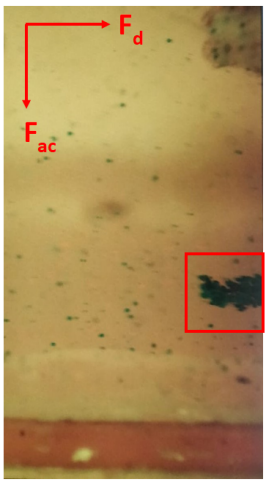

Figure B.4: Aggregation of the larger particles.

C

ADDITIONAL EXPERIMENTS

A few additional experiments were carried out to understand the separation process in the two devices. They have been listed below:

SHAPE OF THE DUAL FREQUENCY ACOUSTIC FIELD:
In order to check if the shape of the acoustic field near the exit was causing the problems mentioned in the previous chapter (refer figure 4.12b), attachments that extended the exit guideway length were added to the device so that shape of the acoustic field at the exits were changed. Two different lengths were tested, one which extended to the middle of the acoustic chamber, and another which altered only the triangular end of the acoustic field. The attachments were 3D printed and attached to the guideway in the device with silicone. In Fig. C.1 the attachments (printed in white) can be seen. Experiments with the attachments revealed that they were not a solution, and the same problems occurred here as well. It might be that the angle of the transducers though help avoid reflections, are not conducive towards separation.

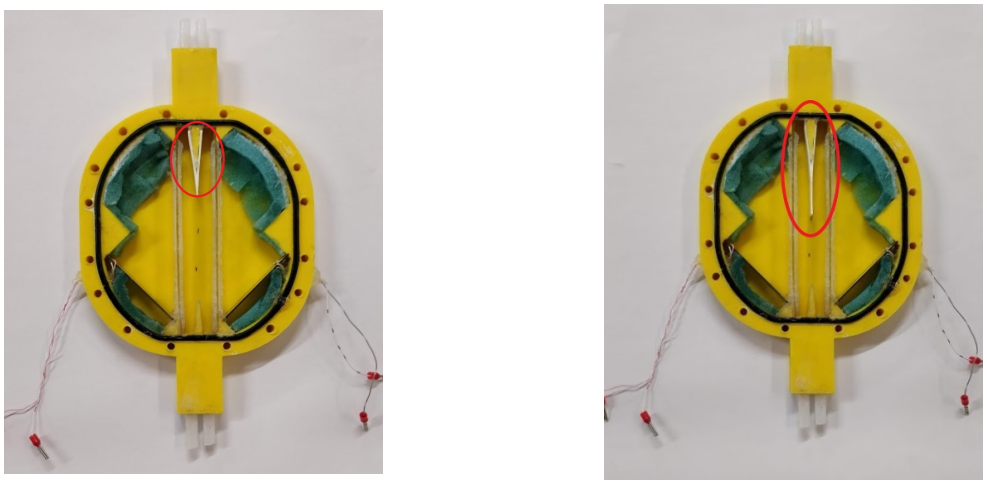

(a) Tip of the acoustic chamber

(b) Mid-length of the acoustic chamber

Figure C.1: Attachments to extend the length of the guideway (circled in red)

ORIENTATION OF DEVICE:
To check if the separation was dependent on gravity, both devices were also tested at two different orientations, in addition to the usual vertical orientation. 1. Horizontal orientation: The device was rotated such that the flow was perpendicular to gravity and the acoustic field was parallel to gravity, 2. Planar orientation: The device was rested on the plane of the table, with flow, acoustic field and gravity being mutually perpendicular. Gravity effects were also added in the simulation models for both devices, with pressure gradient, buoyancy and body forces added in both x & y directions, to

model vertical and the horizontal orientations respectively; the model being 2D precludes modelling the planar orientation.

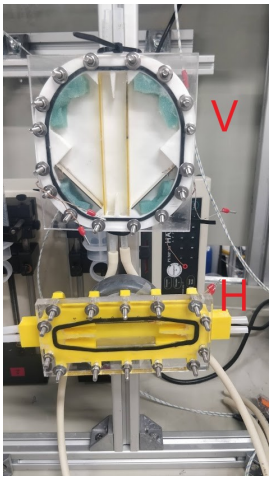

Figure C.2: Representative view of the horizontal & vertical orientations tested

The simulations yielded no change in the threshold sizes for the above mentioned 3 forces, leading to the conclusion that gravity might not be influential in the separation process. In the experiments however, even without the presence of an acoustic field, the particles were seen to be migrating across the channel in both horizontal and planar orientations, while there were no such effects seen in the vertical orientation.
In the dual frequency device in particular, the horizontal orientation had the same in-place oscillation and aggregation of the particles as in the vertical configuration, except that the plane of oscillation was no longer mid-plane but shifted towards the higher-frequency acoustic window. In the planar orientation, no oscillation or aggregation was found, but the migration of particles in the absence of acoustic field still occurred which precluded any possibility of separation. From the above points it is apparent that further study as to the effects of gravity needs to be done.

LOWERING NET CHANNEL FLOW RATE:
To check if the lowered channel flow rate gives rise to better separation purity of the distribution, the channel was operated at a net flow rate of 500 ml h^{-1} in the frequency sweep device. A smaller DOE consisting of 3 flow rates and 2 sweep periods was decided on. The flow rates were split the same way as was done for 1000 ml h^{-1} as: 200 - 300, 225 - 275 & 250 - 250 ml h^{-1}. The applied excitation voltage and sweep periods were subsequently retested for the reduced flow rates. The voltage chosen was the same as the experiments for 1000 ml h^{-1} i.e 25 V_{pp}, but the sweep periods had to be changed and were chosen as 6 & 9 seconds for the larger particles. Around 6 of the experiments were then performed. Pronounced recirculation at the exit guidewary was also noticed in some cases, the causes for which could not be identified. This could be due to the fault of the pump, again indicating a need for a flow meter. The PSD of the transducer and reflector samples also did not indicate any separation.
In the dual frequency device as well, the lowering of channel flow rate was done to check if it changes the working of the device. But the in-plane oscillation and aggregation increased substantially, possibly due to lower drag at the reduced flow rate allowing particles to be trapped much more easily than at the higher flow rate.

Bibliography

[1] Jonathan D Adams, Christian L Ebbesen, Rune Barnkob, Allen HJ Yang, H Tom Soh, and Henrik Bruus. High-throughput, temperature-controlled microchannel acoustophoresis device made with rapid prototyping. *Journal of Micromechanics and Microengineering*, 22(7):075017, 2012.

[2] B Lipkens, J Dionne, A Trask, B Szczur, A Stevens, and E Rietman. Separation of micron-sized particles in macro-scale cavities by ultrasonic standing waves. *Physics Procedia*, 3(1):263–268, 2010.

[3] Gergely Simon, Jose Marques-Hueso, Marc PY Desmulliez, Anne L Bernassau, Dany Roolvink, G Burns, PAG Cormack, Marco AB Andrade, Julien Reboud, Jonathan M Cooper, et al. Reconfigurable particle separation by dynamic acoustic fields in microfluidic devices. In *24th International Conference on Sound and Vibration*, 2017.

[4] Gergely Simon, Yan Pailhas, Marco AB Andrade, Julien Reboud, Jose Marques-Hueso, Marc PY Desmulliez, Jonathan M Cooper, Mathis O Riehle, and Anne L Bernassau. Particle separation in surface acoustic wave microfluidic devices using reprogrammable, pseudo-standing waves. *Applied Physics Letters*, 113(4):044101, 2018.

[5] Jeremy J Hawkes and Stefan Radel. Acoustofluidics 22: Multi-wavelength resonators, applications and considerations. *Lab on a Chip*, 13(4):610–627, 2013.

[6] Phylis WS Pui, Felix Trampler, Stefan A Sonderhoff, Martin Groeschl, Douglas G Kilburn, and James M Piret. Batch and semicontinuous aggregation and sedimentation of hybridoma cells by acoustic resonance fields. *Biotechnology progress*, 11(2):146–152, 1995.

[7] Andreas Lenshof, Cecilia Magnusson, and Thomas Laurell. Acoustofluidics 8: applications of acoustophoresis in continuous flow microsystems. *Lab on a Chip*, 12(7):1210–1223, 2012.

[8] MH Kandemir, RM Wagterveld, DR Yntema, and KJ Keesman. selective particle filtering in a large acoustophoretic serpentine channel. *Scientific reports*, 9(1):1–10, 2019.

[9] Filip Petersson, Lena Åberg, Ann-Margret Swärd-Nilsson, and Thomas Laurell. Free flow acoustophoresis: microfluidic-based mode of particle and cell separation. *Analytical chemistry*, 79(14):5117–5123, 2007.

[10] Jonathan D Adams and H Tom Soh. Tunable acoustophoretic band-pass particle sorter. *Applied physics letters*, 97(6):064103, 2010.

[11] Mitsunori Saito, Norio Kitamura, and Masaki Terauchi. Micro-organism manipulation and microparticle arrangement by the use of ultrasonic standing waves. In *BioMEMS and Smart Nanostructures*, volume 4590, pages 26–37. International Society for Optics and Photonics, 2001.

[12] Albrecht Haake, Adrian Neild, Gerald Radziwill, and Jurg Dual. Positioning, displacement, and localization of cells using ultrasonic forces. *Biotechnology and bioengineering*, 92(1):8–14, 2005.

[13] Patrick Thévoz, Jonathan D Adams, Herbert Shea, Henrik Bruus, and H Tom Soh. Acoustophoretic synchronization of mammalian cells in microchannels. *Analytical chemistry*, 82(7):3094–3098, 2010.

[14] P Augustsson, C Magnusson, C Grenvall, H Lilja, and T Laurell. Extraction of circulating tumor cells from blood using acoustophoresis. In *Micro Total Analysis Systems*, volume 2010, 2010.

[15] Josefina Dykes, Andreas Lenshof, Britt Åstrand-Grundström, Thomas Laurell, and Stefan Scheding. Efficient removal of platelets from peripheral blood progenitor cell products using a novel micro-chip based acoustophoretic platform. *PloS one*, 6(8), 2011.

[16] Jeremy J Hawkes, Robert W Barber, David R Emerson, and W Terence Coakley. Continuous cell washing and mixing driven by an ultrasound standing wave within a microfluidic channel. *Lab on a Chip*, 4(5):446–452, 2004.

[17] Filip Petersson, Andreas Nilsson, Henrik Jönsson, and Thomas Laurell. Carrier medium exchange through ultrasonic particle switching in microfluidic channels. *Analytical chemistry*, 77(5):1216–1221, 2005.

[18] Jeremy J Hawkes and W Terence Coakley. A continuous flow ultrasonic cell-filtering method. *Enzyme and microbial technology*, 19(1):57–62, 1996.

[19] GD Skotis, DRS Cumming, JN Roberts, MO Riehle, and AL Bernassau. Dynamic acoustic field activated cell separation (dafacs). *Lab on a Chip*, 15(3):802–810, 2015.

[20] Moniek Beelen. Travelling acoustic waves for selective particle separation. Master's thesis, Wageningen University & Research, 2019.

[21] Lev Petrovich Gor'kov. On the forces acting on a small particle in an acoustical field in an ideal fluid. In *Sov. Phys. Dokl.*, volume 6, pages 773–775, 1962.

[22] Chwan Bor Fuh, Marcus N Myers, and J Calvin Giddings. Analytical splitt fractionation: rapid particle size analysis and measurement of oversized particles. *Analytical Chemistry*, 64(24):3125–3132, 1992.

[23] Mikkel WH Ley and Henrik Bruus. Continuum modeling of hydrodynamic particle–particle interactions in microfluidic high-concentration suspensions. *Lab on a Chip*, 16(7):1178–1188, 2016.

[24] Martin Gröschl. Ultrasonic separation of suspended particles-part i: Fundamentals. *Acta Acustica united with Acustica*, 84(3):432–447, 1998.

[25] Mikkel Settnes and Henrik Bruus. Forces acting on a small particle in an acoustical field in a viscous fluid. *Physical Review E*, 85(1):016327, 2012.

[26] S Wang, JS Allen, and AM Ardekani. Unsteady particle motion in an acoustic standing wave field. *European Journal of Computational Mechanics*, 26(1-2):115–130, 2017.